



HAL
open science

Competition within low-density bacterial populations as an unexpected factor regulating carbon decomposition in bulk soil

Alexandre Coche, Tristan Babey, Alain Rapaport, Laure Vieublé Gonod, Patricia Garnier, Naoise Nunan, Jean-Raynald de Dreuzy

► To cite this version:

Alexandre Coche, Tristan Babey, Alain Rapaport, Laure Vieublé Gonod, Patricia Garnier, et al.. Competition within low-density bacterial populations as an unexpected factor regulating carbon decomposition in bulk soil. *Soil Biology and Biochemistry*, 2021, 164 (108423), 10.1016/j.soilbio.2021.108423 . insu-03347522v2

HAL Id: insu-03347522

<https://insu.hal.science/insu-03347522v2>

Submitted on 17 Sep 2021 (v2), last revised 23 Nov 2021 (v3)

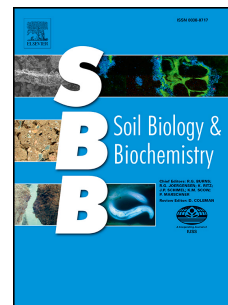
HAL is a multi-disciplinary open access archive for the deposit and dissemination of scientific research documents, whether they are published or not. The documents may come from teaching and research institutions in France or abroad, or from public or private research centers.

L'archive ouverte pluridisciplinaire **HAL**, est destinée au dépôt et à la diffusion de documents scientifiques de niveau recherche, publiés ou non, émanant des établissements d'enseignement et de recherche français ou étrangers, des laboratoires publics ou privés.

Journal Pre-proof

Competition within low-density bacterial populations as an unexpected factor regulating carbon decomposition in bulk soil

Alexandre Coche, Tristan Babey, Alain Rapaport, Laure Vieublé Gonod, Patricia Garnier, Naoise Nunan, Jean-Raynald de Dreuzy



PII: S0038-0717(21)00297-2

DOI: <https://doi.org/10.1016/j.soilbio.2021.108423>

Reference: SBB 108423

To appear in: *Soil Biology and Biochemistry*

Received Date: 16 October 2020

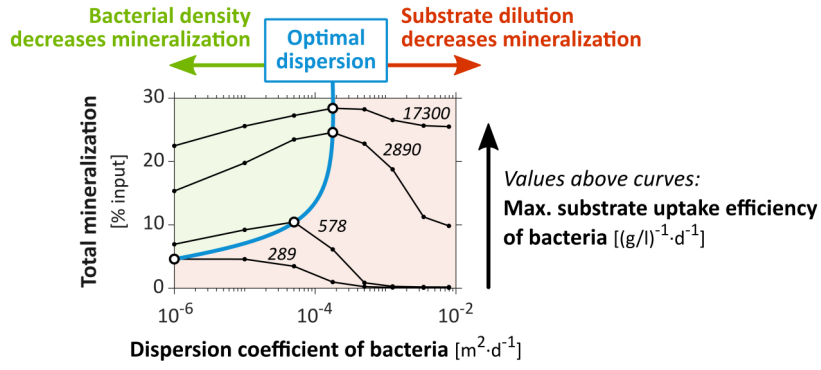
Revised Date: 7 September 2021

Accepted Date: 12 September 2021

Please cite this article as: Coche, A., Babey, T., Rapaport, A., Gonod, L.V., Garnier, P., Nunan, N., Dreuzy, J.-R.d., Competition within low-density bacterial populations as an unexpected factor regulating carbon decomposition in bulk soil, *Soil Biology and Biochemistry*, <https://doi.org/10.1016/j.soilbio.2021.108423>.

This is a PDF file of an article that has undergone enhancements after acceptance, such as the addition of a cover page and metadata, and formatting for readability, but it is not yet the definitive version of record. This version will undergo additional copyediting, typesetting and review before it is published in its final form, but we are providing this version to give early visibility of the article. Please note that, during the production process, errors may be discovered which could affect the content, and all legal disclaimers that apply to the journal pertain.

© 2021 Published by Elsevier Ltd.



1 **Competition within low-density bacterial populations as an**
2 **unexpected factor regulating carbon decomposition in bulk soil**

3 Alexandre Coche^{a*}, Tristan Babey^b, Alain Rapaport^c, Laure Vieublé Gonod^d,
4 Patricia Garnier^d, Naoise Nunan^{e,f}, Jean-Raynald de Dreuzy^a

5 ^a Univ Rennes, CNRS, Géosciences Rennes - UMR 6118, F-35000 Rennes, France

6 ^b Stanford University, Department of Earth System Science, Stanford, USA

7 ^c MISTEA, Univ. Montpellier, INRAE, Montpellier SupAgro, France

8 ^d UMR Ecosys, INRAE, AgroParisTech, Université Paris-Saclay, 78850, Thiverval Grignon,
9 France

10 ^e Sorbonne Université, CNRS, IRD, INRAE, P7, UPEC, Institute of Ecology and Environmental
11 Sciences—Paris, 4 place Jussieu, 75005 Paris, France

12 ^f Department of Soil & Environment, Swedish University of Agricultural Sciences, P.O. Box
13 7014, 75007 Uppsala, Sweden

14 * Corresponding author. *E-mail address*: alexandre.co@hotmail.fr (A. Coche)

15 **Abstract**

16 Bacterial decomposition of organic matter in soils is generally believed to be mainly
17 controlled by the access bacteria have to organic substrate. The influence of bacterial traits
18 on this control has, however, received little attention. Using the concentration-dependent
19 Monod growth model, we develop a bioreactive transport model to screen the interactive
20 impacts of dispersion and bacterial traits on mineralization. Bacterial traits primarily involved

21 in the bacterial response to the substrate concentration, such as the maximum specific
22 uptake rate and efficiency, the adaptation time of the uptake rate and the initial population
23 density, are considered. We compare the model results with two sets of previously
24 performed cm-scale soil-core experiments in which the mineralization of the pesticide 2,4-D
25 was measured under well-controlled initial distributions and transport conditions. Bacterial
26 dispersion away from the initial substrate location induced a significant increase in 2,4-D
27 mineralization. It reveals an increase of specific uptake rates at lower bacterial densities,
28 more than compensating the decrease of specific uptake rates caused by substrate dilution.
29 This regulation of bacterial activities by density, caused by the local depletion of substrate
30 by competing bacteria, becomes dominant for bacteria with an efficient uptake of substrate
31 at low substrate concentrations (a common feature of oligotrophs). Such oligotrophs,
32 commonly found in soils, compete with each other for substrate even at remarkably low
33 population densities. The ratio-dependent Contois growth model, which includes a density
34 regulation in the expression of the uptake efficiency, is more accurate and convenient to
35 calibrate than the substrate-dependent Monod model, at least under these conditions. In
36 view of their strong interactions, bioreactive and transport processes cannot be handled
37 independently but should be integrated, in particular when reactive processes of interest are
38 carried out by oligotrophs.

39 *Keywords:* biodegradation of organic matter; heterogeneous spatial distributions;
40 bioreactive transport model; competition for substrate; bacterial traits; ratio-dependent
41 growth

42 1. Introduction

43 Organic carbon is involved in most ecological functions provided by soils (Bünemann et al.,
44 2018). Its cycling in soil depends upon the activity of microorganisms. Soluble organic
45 molecules are taken up as substrates by specific populations of soil bacteria, and degraded
46 inside the cells by endoenzymes to provide carbon and energy. This is precisely the case for
47 the 2,4-Dichlorophenoxyacetic acid (2,4-D) used in this study as a generic model compound
48 (Don and Weightman, 1985; Pieper et al., 1988; Boivin et al., 2005). Bacterial degradation of
49 soil carbon has generally been modeled with the Monod equation, where the specific
50 substrate uptake rate is controlled by substrate concentration and bacterial traits such as
51 the maximum specific growth rate, the yield (or carbon use efficiency) and the “maximum
52 specific uptake efficiency” (e.g. Monod, 1949; Sinton et al., 1986; Cheyns et al., 2010). With
53 the Monod equation, at the lowest substrate concentration, the specific uptake rate is
54 linearly proportional to the substrate concentration. The proportionality factor is referred to
55 here as the “maximum uptake efficiency” and it reflects the maximal ability of the cell to
56 capture substrate molecules that collide with its membrane (Button, 1978, 1983). The
57 maximum uptake efficiency can also be understood as the volume from which a cell can
58 harvest substrate per unit of time, as used in some studies (Desmond-Le Quéméner and
59 Bouchez, 2014; Nunan et al., 2020; Ugalde-Salas et al., 2020). Each bacterium is assumed to
60 be exposed to the whole substrate concentration of its surroundings, without any limitation
61 by the population density (Lobry and Harmand, 2006).

62 The direct contact (exposure) between bacteria and substrate depends on their spatial
63 distributions (Holden and Firestone, 1997; Nunan et al., 2007). Bacteria and substrate are
64 both heterogeneously distributed as a result of numerous biotic and abiotic processes

65 (Dechesne et al., 2014; Kuzyakov and Blagodatskaya, 2015). There are complex feedback
66 loops between these distributions, dispersive transport processes such as diffusion and
67 hydrodynamic dispersion (Madsen and Alexander, 1982; Breitenbeck et al., 1988), and the
68 bacterial activity itself such as consumption and growth (Poll et al., 2006).

69 Aggregated bacterial distributions, as observed at the mm-scale for 2,4-D degraders (Vieublé
70 Gonod et al., 2003), have been shown to decrease degradation rates when the distribution
71 of substrate is homogeneous, because of local substrate depletion (Pallud et al., 2004;
72 Dechesne et al., 2010). Yet, the role of bacterial metabolic traits on the impact of bacterial
73 and substrate distributions on degradation remains mostly unknown, especially when
74 substrate and bacteria are heterogeneously and dynamically redistributed in soils over
75 μm -to-cm scales by numerous spatial disturbances (Madsen and Alexander, 1982;
76 Breitenbeck et al., 1988; König et al., 2020). We investigated the extent to which bacterial
77 activity and transport processes can be treated independently or should be integrated to
78 characterize, understand and predict degradation under various advective, diffusive and
79 dispersive conditions. The simultaneous characterization of the impacts of bacterial traits
80 and transport parameters through their mutual interactions is methodologically challenging.
81 It requires several well-controlled experiments in comparable degradation conditions, with
82 specific spatial distributions of substrate and degraders in specific transport conditions, and
83 a spatiotemporal monitoring of the different carbon pools.

84 Among the scarce relevant datasets (e.g. Dechesne et al., 2010), we used the two sets of
85 cm-scale soil-core experiments performed by Pinheiro et al. (2015, 2018), in which the
86 degradation of 2,4-D under different initial spatial distributions and transport conditions was
87 measured in similar repacked soil columns. Mostly reported independently, they have shown

88 first that the proximity between bacteria and the initial location of a heterogeneously
89 distributed substrate exerts a strong control on mineralization. Mineralization was greater
90 when bacteria were close to the initial location of substrate, even though most of the initial
91 dissolved substrate diffused away from its initial location. This was attributed to the fact that
92 bacteria located far from the initial substrate location were only exposed to highly diluted
93 substrate concentrations (Babey et al., 2017). However, the hydrodynamic dispersion of
94 both bacteria and substrate away from their initial location caused a greater than four-fold
95 increase in the mineralization of substrate that was not leached out, to the point that it
96 almost reached the same performance as in homogeneous conditions in which there was no
97 dilution (Pineiro et al., 2018). The surprising increase in mineralization suggests a regulation
98 of mineralization by population density compensating the effect of substrate dilution, the
99 activity of bacteria being enhanced when their density is diluted by the dispersive
100 percolation events. While such regulations by bacterial density have not yet been considered
101 in soils, presumably because of the extremely low apparent bacterial densities found in soils
102 (Young et al., 2008), they are well known in bioreactors, where they are usually modeled by
103 the ratio-dependent Contois growth law (Contois, 1959; Harmand and Godon, 2007).

104 In order to determine the relevance of the putative bacterial decomposer density effect on
105 decomposition, we developed a quantitative approach to model the two sets of experiments
106 within the same unified framework (section 2). We assessed the relevance of previously
107 developed models, improved the calibration of a Monod-based model and investigated an
108 alternative Contois-based model (section 3). We discuss the implication of the results on the
109 controlling factors of soil organic carbon cycling, on the relevant bacterial growth models
110 and on the possible bacterial strategies (section 4).

111 **2. Models and methods**

112 ***2.1. Experiment scheme, geometry and initial distributions***

113 We briefly introduce the experiments performed previously and highlight aspects of the
114 experiments that are important for the modeling (**Fig. 1**). The full experimental setting is
115 presented in the supplementary materials (**Fig. S1** and **Table S1**) for the sake of
116 completeness. Soil columns were packed with two homogeneous or heterogeneous
117 arrangements of soil cubes, either sterilized, or hosting the indigenous microbial
118 communities (referred to as “degraders”) and amended with ^{14}C -labelled 2,4-D (referred to
119 as “substrate”). Two sets of experiments, referred to as “hydrostatic” and “percolation”
120 conditions, were performed respectively with only substrate diffusion (Pineiro et al., 2015),
121 or with additional substrate and bacterial advection and dispersion caused by water
122 percolation (Pineiro et al., 2018). The initial locations of the bacteria and substrate were
123 set in the model according to the experimental conditions (**Fig 1A**). Initial concentrations
124 used in the model are detailed in **Table 1**. In the experiments, the mass of mineralized ^{14}C
125 derived from the degradation of the labelled 2,4-D was monitored at the core scale during
126 at least two weeks (**Fig. 1B**). These data were used to confront the model processes with a
127 physical system, as detailed in section 2.5.

128 ***2.2. Bioreactive model***

129 The bioreactive model extends the model published by Babey et al. (2017) (**Fig. 2**) to account
130 for Contois growth law as an alternative to Monod’s. The sorption processes, the bacterial
131 lag phase and the biomass recycling described below were previously discussed and their

132 use justified in Babey et al. (2017) to consistently represent the experimental data. The $r(\cdot)$
 133 notation expresses the reaction rates of the biochemical dynamics that are expressed as
 134 follows:

$$r(S) = k_{AS} A - k_{SA} S - k_R S - \frac{\mu}{y} B + m_t \chi B \quad (1)$$

$$r(A) = k_{SA} S - k_{AS} A \quad (2)$$

$$r(R_S) = k_R S \quad (3)$$

$$r(CO_2) = \frac{(1-y)}{y} \mu B \quad (4)$$

$$r(B) = \mu B - m_t B \quad (5)$$

$$r(R_B) = m_t(1-\chi)B \quad (6)$$

135 All variable and parameter definitions are listed in **Table 1**. The dynamics of the specific
 136 growth rate μ are given, for the Monod-based model, by:

$$\frac{\partial \mu}{\partial t} = \alpha \left(\mu_{max} \frac{S}{\kappa_M + S} - \mu \right) \quad (7)$$

137 and, for the Contois-based model, by:

$$\frac{\partial \mu}{\partial t} = \alpha \left(\mu_{max} \frac{S/B}{\kappa_C + S/B} - \mu \right) = \alpha \left(\mu_{max} \frac{S}{\kappa_C B + S} - \mu \right) \quad (8)$$

138 where $\mu = 0$ at $t = 0$.

139 The dissolved substrate S is either reversibly adsorbed to soil particles (pool A) or irreversibly
 140 adsorbed (pool R_S) (Eqs. (1), (2), (3)), or taken up by bacteria B (Eq. (1)) and metabolized into
 141 CO_2 (Eq. (4)) and new biomass B (Eq. (5)). k_{SA} and k_{AS} are the reversible sorption coefficients.
 142 k_R is the irreversible one. Bacteria death occurs at a constant rate m_t (Eq. (5)) and a fraction
 143 of the bacterial necromass is considered to return to the dissolved substrate pool S to
 144 account for biomass recycling (Eq. (1)), while the rest is transformed to biotic residues R_B
 145 (Eq. (6)). The remobilization of carbon previously absorbed by bacteria is necessary to

146 adequately predict the slower dynamics of mineralization that takes place once most of the
147 dissolved substrate has been consumed, observed after 5 days in homogeneous experiments
148 and after respectively 3 or 10 days in the heterogeneous hydrostatic or percolation
149 experiments. This remobilization is modeled in the form of a biomass recycling in order to
150 be consistent with the model previously published in Babey et al. (2017), but similar effects
151 could be achieved by other mechanisms, like a slower mineralization of biogenic residues
152 (**Fig. S9**). Its impact on the final mineralization does not account for more than 10% of the
153 substrate that is not leached out. The adsorbed substrate and biotic residues form the pool
154 of insoluble carbon $A + R_S + R_B$. The substrate S is consumed by bacteria B according to their
155 specific uptake rate $(1/y) \cdot \mu$ expressed either by the substrate-dependent Monod growth law
156 (Eq. (7)) (Monod, 1949) or by the ratio-dependent Contois growth law (Eq. (8)) (Contois,
157 1959). y is the yield coefficient and relates the specific uptake rate $(1/y) \cdot \mu$ to the specific
158 growth rate μ . μ_{max} is the maximum specific growth rate. κ_M and κ_C are Monod and Contois
159 constants respectively. The effective uptake is delayed by the accommodation rate α , which
160 explicitly takes into account the “memory” effects of the bacteria when adapting to new
161 conditions (Patarinska et al., 2000). This delay is necessary to capture the mineralization lag
162 time at the beginning of the experiments (see **Fig. S10**). Over long time periods ($t \gg 1/\alpha$), μ
163 follows the exact expression of the Monod or Contois equations. All modeled pools (S , B ,
164 CO_2 , A , R_S and R_B) were expressed as carbon concentrations in $\mu\text{g}\cdot\text{g}^{-1}$ (mass of carbon per
165 mass of dry soil) considering a soil water content of $0.205 \text{ g}\cdot\text{g}^{-1}$ (mass of water per mass of
166 dry soil), a bulk density of the soil column of $1.3 \cdot 10^3 \text{ g}\cdot\text{l}^{-1}$ (mass of dry soil per apparent soil
167 volume) and an average bacterial dry weight of $2.8 \cdot 10^{-13} \text{ g}$ corresponding to $1.49 \cdot 10^{-13} \text{ g}$ of
168 carbon per cell. These values of water content and bulk density were those set up in the
169 experiments, the latter corresponding to a water potential adjusted at -31.6 kPa (pF 2.5).

170 The average bacterial weight was assumed based on Dechesne et al. (2010) and Pinheiro et
 171 al. (2015). The water-filled pore space (54%, volume of water per volume of pores) was such
 172 that oxygen was not considered a limiting factor for 2,4-D degradation.

173 **2.3. Reactive transport model**

174 The transport model is based on the diffusion model of Babey et al. (2017) to which
 175 advective-dispersive processes explored in the experiments of Pinheiro et al. (2018) are
 176 added. Bacterial leaching out and dispersion were observed only in the percolation
 177 experiments while the substrate was also reported to diffuse. Hydrodynamic leaching and
 178 dispersion were modeled independently, as they result from, respectively, bypass flow
 179 through large pores and complex hydrodynamic dispersion processes coming not only from
 180 usual flow mechanisms but also from large saturation variations and local redistribution of
 181 moisture in the pore network. Due to the lack of adequate experimental data to characterize
 182 the details of the dispersion process, we applied a simple isotropic dispersion coefficient.
 183 Complementary numerical simulations show that other anisotropic dispersion
 184 parameterization are only weakly sensitive (**Fig. S3** and **S4**). Bacterial and substrate
 185 transports were described with the same advective and dispersive parameters. This
 186 assumption did not significantly alter the results (**Fig. S5** and **S6**). Coupled to the equations
 187 of the bioreactive model ((1)-(8)), the full reactive transport model is given by:

$$\frac{\partial S}{\partial t} = r(S) + \nabla(d_{diff}\nabla S) + G(\nabla(d_{disp}\nabla S) - v S) \quad (9)$$

$$\frac{\partial B}{\partial t} = r(B) + G(\nabla(d_{disp}\nabla B) - v B) \quad (10)$$

$$\frac{\partial U}{\partial t} = r(U) \quad \text{for } U = A, R_B, R_S \text{ and } CO_2 \quad (11)$$

188 where d_{diff} is the effective molecular diffusion coefficient of S , d_{disp} is the effective
 189 hydrodynamic dispersion coefficient of S and B and v is their leaching rate. Note that the
 190 dispersion coefficient d_{disp} mostly affected the spreading of bacteria, given that substrate
 191 was mainly spread by diffusion, as noted in section 2.3 and confirmed by consistent results
 192 from equivalent models without hydrodynamic dispersion of S (**Fig. S7** and **S8**). Effective
 193 diffusion and dispersion processes were assumed to be isotropic and uniform at the
 194 column-scale. Dispersion and leaching were active only during the observed 1-hour
 195 percolation events at days 0, 3 and 6 as controlled by the function G defined as:

$$G(t) = 1 \quad t = [0d - 0d1h]; [3d - 3d1h]; [6d - 6d1h] \quad (12)$$

$$G(t) = 0 \quad \text{otherwise.}$$

196 No-flow boundary conditions were imposed at the edges of the soil core ($\nabla S = 0$ and $\nabla B = 0$)
 197 during periods outside of the percolation events. The transient evolutions of the water
 198 content and their effects on concentrations were not considered because of the short
 199 duration of the percolation events (1 h) and the absence of detectable effects on the
 200 experimental mineralization curve around the percolation events (**Fig. 1D**). Hydration
 201 conditions were considered constant, constrained by the water potential adjusted
 202 to -31.6 kPa. No bacterial mobility was observed in the hydrostatic experiments, suggesting
 203 that the bacterial mobility observed in the percolation experiments resulted primarily from
 204 hydrodynamic dispersion.

205 Carbon pools concentration dynamics were simulated on a $3 \times 6 \times 6$ regular mesh grid.

206 Although the shape of the grid was slightly different from that of the cylindrical soil-core, it

207 did not have any observable impact (Babey et al., 2017). We recall that substrate and
208 bacteria were initially co-located in the same cube(s). Each cube was considered to be
209 physically, chemically and biologically homogeneous. Diffusion and dispersion were
210 simulated using a finite-difference scheme (Iserles, 2009) and coupled with the bioreactive
211 model, itself solved by the 4th order Runge-Kutta integration method function of MATLAB
212 (Shampine and Reichelt, 1997). The coupling of transport and bioreactive models was
213 achieved with a sequential non-iterative operator-splitting method, in which the equations
214 are resolved within each time step in a sequence of one transport step followed by one
215 bioreactive step (Carrayrou et al., 2004; Lagneau and van der Lee, 2010). The time steps were
216 smaller than the characteristic diffusion and reaction times to avoid any coupling issues.

217 **2.4. Exploratory screening**

218 Parameters and their values are listed in **Table 1**. Sorption parameters and the diffusion
219 coefficient were set at values that were calibrated and validated by Babey et al. (2017) in
220 independent experiments without degradation. The mortality rate and the biomass recycling
221 yield were also kept at the values calibrated in Babey et al. (2017) as they were considered
222 to be well constrained by the residual mineralization dynamics of the homogeneous
223 hydrostatic experiment (**Fig. 1D**). The four biological parameters primarily involved in the
224 biological response of bacteria to the concentration of substrate were determined to be
225 $(1/y) \cdot \mu_{max}$, α , $B(t=0)$ and either $(1/y) \cdot \mu_{max}/K_M$ for the Monod-based model or
226 $(1/y) \cdot \mu_{max}/(B(t=0) \cdot \kappa_C)$ for the Contois-based model. Each of these four parameters were
227 sampled over 7 logarithmically-distributed values within the theoretically and physically
228 relevant ranges given by Babey et al. (2017), and all possible combinations of values were

229 screened (**Table S2**). We recall that the “maximum uptake efficiency” $(1/y) \cdot \mu_{max} / \kappa_M$
230 characterizes the specific bacterial uptake of substrate at the lowest substrate concentration
231 (Button, 1991), while the maximum specific uptake rate $(1/y) \cdot \mu_{max}$ characterizes the
232 bacterial uptake at the highest substrate concentration. Note that the uptake yield y was
233 fixed at the value calibrated by Babey et al. (2017) with a high degree of certainty. The initial
234 maximum uptake efficiency $(1/y) \cdot \mu_{max} / (B(t=0) \cdot \kappa_C)$ in the Contois-based model was
235 screened in the same range as $(1/y) \cdot \mu_{max} / \kappa_M$. The accommodation rate α of the degrader
236 response ranged from a negligible delay of few minutes ($\alpha = 934 \text{ d}^{-1}$) to a prolonged delay of
237 around 10 days ($\alpha = 9.34 \cdot 10^{-2} \text{ d}^{-1}$). $B(t=0)$ values were screened around the initial
238 experimental measurements of the *tfdA* gene copy number, assuming that one *tfdA*
239 sequence corresponded to one bacterium. They ranged over two orders of magnitude to
240 account for the uncertainty of the conversion of *tfdA* copy number into alive 2,4-D degraders
241 (Bælum et al., 2006, 2008). Bacterial density in the uptake efficiency expression will also be
242 expressed in $\text{g} \cdot \text{l}^{-1}$ (mass of bacteria per volume of water) for a more direct comparison with
243 the relevant literature.

244 The spatial distribution of bacteria observed at the end of the experiments could not be used
245 to determine the effective dispersion coefficient d_{disp} (**Fig. S2**). While they qualitatively
246 ascertained that bacteria spread orthogonally to the percolation direction, experimental
247 data were not sufficiently resolved to be used quantitatively. The dispersion coefficient was
248 thus screened over 10 values ranging from no dispersion ($d_{disp} = 0$) to complete instant
249 homogenization of the soil core ($d_{disp} = \text{inf}$) (**Table S2**). In order to analyze the result of
250 bacterial dispersion in terms of distance from the initial location of the substrate, we
251 compute the root-mean-square displacement of bacteria, defined as the root-mean-square

252 of their spreading during the duration Δt of one percolation event and expressed as
 253 $\sqrt{6 d_{disp} \Delta t}$ (Stana, 2020). The effective diffusion coefficient d_{diff} had been calibrated
 254 independently from percolation conditions (Pineiro et al., 2015; Babey et al., 2017). The
 255 leaching rates v were determined based on the experimental masses of leached ^{14}C (Pineiro
 256 et al., 2018) (**Table 1**). Detailed values for the screened parameters are listed in **Table S2**.

257 **2.5. Model to data comparison**

258 The comparison between the results of the model and the experimental data was based on
 259 the core-scale data of mineralization deduced from the carbon mass m_{CO_2} of $^{14}\text{CO}_2$ emissions:

$$m_{CO_2}(t) = \int_V CO_2(x, t) dx \quad (13)$$

260 with V the volume of the soil cores. Mineralization at a given time t was expressed as the
 261 carbon mass of cumulated $^{14}\text{CO}_2$ emissions ($m_{CO_2,q}(t)$) per initial carbon mass of
 262 ^{14}C -substrate S ($m_{S,q}(t=0)$) where the index q identifies the experiment at hand. Indices
 263 1, 2, 3 and 4 are respectively given to the homogeneous hydrostatic, heterogeneous
 264 hydrostatic, homogeneous percolation and heterogeneous percolation experiments.
 265 Data-to-model adequacy was assessed for each of the experiments by a classical root-mean-
 266 square evaluation function J_q comparing the modeled mineralization of Eq. (4) to the
 267 measured mineralization at the n_q available sampling times t_i :

$$J_q = \left(\frac{1}{n_q} \sum_{i=1}^{n_q} \left(\frac{m_{CO_2,q}^{mod}(t_i) - m_{CO_2,q}^{data}(t_i)}{m_{S,q}(t=0)} \right)^2 \right)^{\frac{1}{2}} \quad (14)$$

268 Discrepancies over the full set of experiments J_{1234} were thus expressed as:

$$J_{1234} = \left(\frac{1}{4} \sum_{k=1}^4 J_k^2 \right)^{\frac{1}{2}} \quad (15)$$

269 Following the systematic parameter screening described in section 2.4, the parameter set
 270 minimizing J_{1234} was determined and referred to as the set calibrated on both hydrostatic
 271 and percolation experiments. The measurement errors were in average 1.7 times higher in
 272 the percolation experiments than in the hydrostatic experiments. This was assumed to be
 273 due to differences in experimental setup between the two sets of experiments of Pinheiro
 274 et al. (2015, 2018). This error difference contributed to limit the weight of the percolation
 275 experiments when determining the best-fitting parameter set over the whole set of
 276 experiments (J_{1234}). We made the choice to give an equal weight to all experiments by only
 277 taking into account the average CO₂ values.

278 **3. Results**

279 **3.1. Model calibration**

280 The calibration of the bioreactive transport model carried out using only the hydrostatic
 281 experimental data (Babey et al., 2017) led to a minimal discrepancy between data and model
 282 of $J_{12} = 0.023$ (**Fig. 3-A1 and A2**). This pre-existing parameterization was used to provide blind
 283 predictions of the percolation experiments, with the effective dispersion coefficient d_{disp} as
 284 an additional fitting parameter. It gave a reasonable prediction of mineralization in the
 285 homogeneous percolation experiment ($J_3 = 0.038$, **Fig. 3-A3**) but failed in the heterogeneous
 286 percolation experiment ($J_4 = 0.151$, **Fig. 3-A4**), regardless of the dispersion coefficient values.

287 The smallest discrepancy J_4 was surprisingly obtained without any bacterial dispersion
288 ($d_{disp} = 0$) in contradiction with the bacterial spread observed in the experimental data
289 (**Fig. S2**). The final predicted mineralization was highest when bacteria remained aggregated
290 close to the initial location of the substrate. The highest predicted mineralization was
291 however four times lower than the experimental data. The large gap between the
292 experimental data and the modeled scenario suggests that bacterial proximity to the initial
293 substrate location is not the underlying explanatory mechanism for the high mineralization
294 rates. On the contrary, it suggests that mineralization might rather be increased by the
295 dispersion of bacteria towards more diluted substrate concentrations, and that the identified
296 bacterial traits do not match this increase of mineralization with dispersion.

297 In order to investigate the capacity of the reactive transport model to fit both hydrostatic
298 and percolation experimental data, the biological parameters ($(1/y) \cdot \mu_{max}/\kappa_M$, $(1/y) \cdot \mu_{max}$, α ,
299 $B(t=0)$) and the dispersion coefficient (d_{disp}) were calibrated on both hydrostatic and
300 percolation experiments following the screening approach given in section 2.4 to minimize
301 J_{1234} . The mineralization dynamics were adequately predicted in all four experiments with
302 the biological parameter set giving the lowest overall discrepancy ($J_{1234} = 0.032$) and a
303 non-zero dispersion coefficient ($d_{disp} = 1.78 \cdot 10^{-4} \text{ m}^2 \cdot \text{d}^{-1}$) (**Fig. 3, Table 2**). The non-zero
304 dispersion coefficient indicates that the calibrated model accounts for a positive impact of
305 bacterial dispersion on degradation. The model results suggest that this effect is necessary
306 to successfully predict the high degree of degradation in the experimental data. Compared
307 to the parameters calibrated only using the hydrostatic experiments, the parameter set
308 calibrated on both hydrostatic and percolation experiments also displayed a much higher
309 maximum uptake efficiency $(1/y) \cdot \mu_{max}/\kappa_M = 26.5 \text{ g} \cdot \mu\text{g}^{-1} \cdot \text{d}^{-1}$ (mass of dry soil per mass of

310 bacterial carbon per unit of time) (**Table 2**). The systematic exploration of the parameter
311 space showed that high maximum uptake efficiency was a common feature of the 1%
312 best-fitting parameterizations over both hydrostatic and percolation experiments (smallest
313 J_{1234}), with values of 159 and $26.5 \text{ g} \cdot \mu\text{g}^{-1} \cdot \text{d}^{-1}$, corresponding respectively to $1.73 \cdot 10^4$ and
314 $2.89 \cdot 10^3 \text{ l} \cdot \text{g}^{-1} \cdot \text{d}^{-1}$ (volume of water per mass of bacteria per unit of time). It underlines the
315 essential role of the maximum uptake efficiency for modulating the impact of dispersion on
316 degradation, further detailed and explained in section 3.2.3.

317 **3.2. Analysis of the controls exerted on degradation by substrate dilution and** 318 **bacterial density**

319 The effect of dispersion on degradation differed greatly between the two calibrated sets of
320 biological parameters described in section 3.1. We therefore conducted a more systematic
321 investigation of the coupled impact of bacterial dispersion and bacterial traits on
322 degradation, revealing its control by substrate dilution and bacterial density.

323 **3.2.1 Impact of dispersion on degradation**

324 We used the mineralization at the end of the experimental time (day 24) as a proxy for
325 degradation and determined its sensitivity to dispersion, as a function of the
326 parameterization of bacterial traits. **Fig. 4** shows the impact of the dispersion coefficient d_{disp}
327 on the final predicted mineralization for the two calibrated biological parameter sets, all
328 other parameters being kept constant (thick red and blue lines). For the biological parameter
329 set calibrated on hydrostatic experiments, the final mineralization decreased monotonically
330 with dispersion (**Fig. 4**, red line). For the parameter set calibrated on both hydrostatic and
331 percolation experiments, the final mineralization first increased, reached a maximum around

332 $d_{disp} \approx 10^{-4} \text{ m}^2 \cdot \text{d}^{-1}$ and then decreased (**Fig. 4**, blue line). These two kinds of behaviors were
333 observed regardless of the parameters α , $(1/y) \cdot \mu_{max}$ and $B(t=0)$ as long as $(1/y) \cdot \mu_{max} / \kappa_M$
334 remained the same (**Fig. S12**). The non-monotonic impact of dispersion on degradation
335 highlights the existence of an optimal bacterial dispersion for which mineralization is the
336 highest. The comparison between the red and blue lines on **Fig. 4** suggests that the optimal
337 dispersion value depends on the bacterial uptake efficiency. Note that, although the optimal
338 dispersion value varied with time due to the spatial dynamics of both bacteria and substrate
339 (**Fig. S14**), it tended towards a limit that was mostly reached within 4 to 7 days and is thus
340 represented at day 24 on **Fig. 4**.

341 3.2.2 *Double control of degradation by substrate dilution and bacterial density*

342 The non-monotonic effect of bacterial dispersion on degradation is an unusual and key
343 feature of the model calibrated on both hydrostatic and percolation experiments. In the
344 following we will present an explanation for how such relationships between dispersion and
345 degradation could arise, resulting from a non-monotonic spatial substrate profile, itself
346 derived from the respective effects of substrate dilution and bacterial density.

347 In the model, the instant exposure of bacteria to their substrate is maximal if all the bacteria
348 are located inside the voxel(s) with the highest substrate concentration. In the hydrostatic
349 calibrated parameter set, the profile of substrate concentration primarily resulted from its
350 initial heterogeneity (bell-shape red curve on **Fig. 5A** and pseudo bell-shape red curve on
351 **Fig. 5B**). The flux of substrate reaching each bacterium was therefore mostly determined by
352 the distance between the bacterium and the initial location of substrate. The exposure of a
353 single bacterium to the substrate decreased with its distance from the substrate initial
354 location. This effect is referred to as “substrate dilution”. In these cases (**Fig. 5A and B**),

355 mineralization was mainly regulated by substrate dilution, and therefore reduced by
356 bacterial dispersion (**Fig. 4**, blue line). However, for the parameter set calibrated on both
357 hydrostatic and percolation experiments, local degradation by aggregated bacteria reshaped
358 the substrate spatial profile, thus critically changing the voxel(s) with the highest substrate
359 concentration. The bacteria aggregated at their initial location consumed the substrate much
360 faster than it was replenished by backward diffusion and dispersion, creating a critical
361 inversion of the substrate gradient, which led to an intra-population competition for
362 substrate (**Fig. 5C**). The competition was critical for bacterial densities as small as $3.5 \cdot 10^{-3}$
363 $\text{g}\cdot\text{l}^{-1}$ (**Fig. 5C**). In contrast, the dispersion of bacteria reduced competition by diluting the
364 highest bacterial densities, thus flattening the substrate gradient inversion induced by
365 bacterial local degradation, resulting in a better overall exposure of bacteria to the substrate
366 concentrations, and thus an enhanced mineralization (**Fig. 5D**). In these cases (**Fig. 5C** and
367 **D**), mineralization was mainly regulated by bacterial density, or in other words by the
368 distances among bacteria. The relationship between bacterial density and the limitation of
369 their exposure to the substrate is not instantaneous and is mediated by the local depletion
370 of the substrate concentration. This is expressed in the model equations through the
371 dependence of bacterial activity $\mu(t)$ on substrate concentration $S(t)$ (Eq. (7)) and the
372 dependence of the substrate concentration $S(t)$ on degradation $\mu(t)\cdot B(t)$ (Eq. (1)), within
373 each voxel. However, when bacterial dispersion was too great, substrate dilution became
374 the dominant control again. This suggests that an optimal bacterial spatial spread exists for
375 which the dilution of substrate is compensated by the dilution of high local bacterial
376 densities. The modeled scenario illustrated by the two calibrated parameter sets were also
377 observed for most of the other parameter sets. The optimal dispersion coefficient for the
378 300 best-fitting parameterizations to both hydrostatic and percolation experiments (smallest

379 J_{1234} values) was on average $d_{disp} \approx 2 \cdot 10^{-5} \text{ m}^2 \cdot \text{d}^{-1}$ (**Fig. S15**), corresponding to a
380 root-mean-square displacement of bacteria of 1.5 to 3.5 mm during each percolation event.

381 3.2.3 Effect of bacterial uptake efficiency on the impact of dispersion on degradation

382 A non-monotonic substrate concentration profile only occurs when bacterial degradation
383 locally depletes the substrate faster than it is replenished by diffusion. This area of high local
384 competition for substrate results from either high local densities of bacteria or high
385 competitiveness or both. Bacterial competitiveness is related to their maximum uptake
386 efficiency $(1/y) \cdot \mu_{max}/K_M$, which also describes their capacity to maintain their activity and
387 growth under dilute substrate concentrations (Healey, 1980; Button, 1991; Lobry et al.,
388 1992). Bacteria with high maximum uptake efficiency are thus expected to benefit more
389 from dispersion. **Fig. 6** shows the optimal dispersion coefficient as a function of the
390 maximum uptake efficiency, with all other parameters equal to those of the model calibrated
391 on both hydrostatic and percolation experiments. The optimal dispersion coefficient,
392 defined as the dispersion coefficient maximizing the final mineralization, increased with the
393 maximum uptake efficiency. For small maximum uptake efficiencies of $30 \text{ l} \cdot \text{g}^{-1} \cdot \text{d}^{-1}$ and below,
394 mineralization was highest in the absence of dispersion, suggesting a regulation dominated
395 by substrate dilution. For larger maximum uptake efficiencies, dispersion impacted positively
396 mineralization, suggesting that degradation shifted from being regulated by substrate
397 dilution to being regulated by bacterial densities, as bacteria were both more prone to
398 competition between themselves and more efficient under diluted substrate conditions. In
399 other words, the proximity to other bacteria constrained activity more than the proximity to
400 the substrate initial location enhanced it. This combined effect of the maximum uptake

401 efficiency and the bacterial dispersion on degradation was a general relationship common
402 to all parameterizations (**Fig. S16**).

403 **3.3. The Contois-based model as an alternative to Monod**

404 Given that degradation is regulated by both substrate dilution and bacterial density, and that
405 their relative importance is modulated by bacterial uptake efficiency at the lowest substrate
406 concentration, $(1/y) \cdot \mu_{max}/\kappa_M$, we investigated the relevance of the Contois model by
407 applying the calibration methodology of section 2.5, as used in section 3.1. The interest in
408 the Contois growth law (Eq. (8)) stems from the inclusion of a regulation by density in the
409 expression of the uptake efficiency at the lowest substrate concentration, becoming
410 $(1/y) \cdot \mu_{max}/(B(t) \cdot \kappa_C)$.

411 In comparison with the Monod-based model, the predictions of the experimental
412 observations of Pinheiro et al. (2015, 2019) were facilitated with the Contois-based model,
413 on three levels. First, the Contois-based model captured the degradation dynamics better
414 than the Monod-based model, especially for the 1% best-fitting parameterizations (smallest
415 J_{1234} values) (**Fig. S17**). The calibrated Contois-based model had an overall discrepancy of
416 $J_{1234} = 0.022$ (**Fig. 7**), which was smaller than the lowest value of $J_{1234} = 0.032$ obtained for
417 the calibrated Monod-based model (**Fig. 3**). Second, the parameter sets that fitted
418 homogeneous experiments also performed well under heterogeneous conditions, as long as
419 the dispersion coefficient d_{disp} was calibrated as well (**Fig. S18**). It is an important advantage
420 as it confers a better capacity to predict degradation kinetics for heterogeneous and varying
421 distributions, once the model is calibrated in homogeneous conditions, which are more
422 appropriate for the experimental measurement of bacterial parameters. Besides, using a

423 dispersion coefficient value different from the calibrated one weakened the predictions of
424 the mineralization dynamics but not the predictions of the mineralization after 24 days,
425 which remained satisfying regardless of the dispersion coefficient. More precisely, the
426 prediction of the final mineralization became mostly independent of the dispersion
427 coefficient, as shown for the calibrated model (**Fig. 8**). This is because, in the Contois model
428 at low substrate concentrations, the number of active bacteria in a soil volume is exactly
429 counterbalanced by the regulation of their uptake efficiency by population density (Eq. (8)),
430 resulting in limited effects of bacterial spreading on overall mineralization (**Fig. 8**, constant
431 part of the curves).

432 **4. Discussion**

433 ***4.1. Relevance of density control for 2,4-D degradation and soil carbon cycling***

434 *4.1.1 Density control of soil oligotroph bacteria*

435 Bulk soil and highly-diluted environments are usually found to be dominated by bacteria with
436 high maximum uptake efficiency, also called oligotrophs (Fierer et al., 2007; Nunan et al.,
437 2020). Their high maximum uptake efficiency differentiates their life-history strategies and
438 conditions their ability to thrive in resource poor environments (Button, 1993), also
439 assimilated to K-strategy (Tecon and Or, 2017), by opposition to copiotrophic bacteria
440 adapted to rich environments (r-strategy). The maximum uptake efficiency values of the 1%
441 best-fitting parameter sets were of the order of 10^3 - 10^4 l·g⁻¹·d⁻¹ (volume of water per mass
442 of bacteria per unit of time), within the range proposed by Button (1991) to define
443 oligotrophs. Similar or higher maximum uptake efficiency values of the order of

444 10^4 - 10^5 l·g⁻¹·d⁻¹ have been reported for soil oligotrophs (Ohta and Taniguchi, 1988; Zelenev
445 et al., 2005). Values up to $1.64 \cdot 10^5$ have been reported by Tuxen et al. (2002) for 2,4-D
446 degraders in an aerobic aquifer and even greater values might also be possible (see section
447 S5). The high maximum uptake efficiencies predicted in section 3.1 for the best-fitting
448 parameterizations are therefore a plausible bacterial trait among 2,4-D degraders as well as
449 bulk soil bacteria in general. It suggests that density control might be relevant for a
450 component of soil bacteria, which would benefit from dispersion as suggested by **Fig. 6**. The
451 calibrated model has shown in section 3.2.2 that the values of densities from which
452 competition became critical were around $3.5 \cdot 10^{-3}$ g·l⁻¹, corresponding to $7.5 \cdot 10^{-7}$ g·g (mass of
453 bacteria per mass of dry soil), ranging in the low end of usual total soil bacterial densities
454 (Raynaud and Nunan, 2014; Kuzyakov and Blagodatskaya, 2015). This suggests that
455 competition might play a significant role even under the low bacterial densities observed in
456 bulk soils, at least in similar substrate conditions. Reciprocally, the model suggests that
457 competition for substrate between copiotrophic bacteria only appears at much larger
458 population densities, such as those found in soil biofilms (Holden et al., 1997, Or et al., 2007).
459 Interestingly, copiotrophic bacteria have been reported to cohabit with oligotrophic bacteria
460 even in diluted environments (Gözdereliler et al., 2012). Results from the screening suggest
461 that, for densities of copiotrophs as low as for oligotrophs, their impact on overall
462 decomposition in dilution-dominated environments would be much lower due to their
463 poorly adapted uptake efficiency (**Fig. 4A**). Conversely, this striking density regulation might
464 be one of the main limitations of the overall population densities in soils. Note that this
465 density regulation occurs within a single population with homogeneous biological constants.
466 Spatial heterogeneities and low substrate concentrations, common in bulk soil, may indeed

467 shift competition from the inter-population level to the intra-population level (Pfeiffer et al.,
468 2001; Roller and Schmidt, 2015).

469 *4.1.2 A new perspective on Regulatory Gate hypothesis*

470 Density regulation might partially contribute to explain the common paradox of the apparent
471 uncoupling between the overall mineralization of a soil volume and the size of its microbial
472 population (Kemmitt et al., 2008). The rate of soil carbon mineralization remains the same
473 even if 90% of the microbial decomposers are killed. This observation is commonly explained
474 by the Regulatory Gate hypothesis, where mineralization is assumed to be controlled by an
475 abiotic process, such as desorption or diffusion, that limits the availability of the substrate,
476 resulting in mineralization rates that are independent of the degrader abundance. We
477 propose that the density regulation of decomposition in oligotrophic environments may
478 contribute to this phenomenon, through competition for substrate or other biological
479 interactions. In the case of competition-related density regulation, it reduces the
480 dependence of the overall carbon mineralization on degrader abundance, as any increase of
481 population density counterbalances the effect of the increased population size. Note that
482 the involved abiotic process, namely the substrate diffusion backward to bacteria (see
483 section 3.2), is well limiting but only in situations of high bacterial competition.

484 **4.2. Relevance of the ratio-dependent Contois model in soils**

485 As argued in section 3.3, ratio-dependence might facilitate decomposition modeling in the
486 soil conditions typical of the experiments analyzed here. The Contois model's $(1/y) \cdot \mu_{max}/\kappa_{CB}$
487 calibrated in homogeneous conditions might be used in heterogeneous conditions more
488 reliably than the Monod model's $(1/y) \cdot \mu_{max}/\kappa_M$, at least for soil systems in which the

489 competition for the substrate plays a substantial role within the degrader population. The
490 similarity between κ_M and κ_{CB} suggests the need to consider population density when
491 measuring the apparent maximum uptake efficiency of soil bacteria to avoid
492 underestimating it by unintentionally including density regulation. Moreover, the better
493 predictions obtained with the Contois model in the soil conditions represented by the
494 experiments suggest that the Contois ratio-dependence includes not only the effect of
495 competition for substrate at the scale of measurement, but it can also reasonably reflect
496 other density processes such as the spatial variability of bacterial distributions at finer scales
497 related to their high degree of local aggregation in microcolonies (Raynaud and Nunan,
498 2014). Moreover, ratio-dependence may also include the cumulative effects of ecological
499 interactions other than competition (Sibly and Hone, 2002). Note that the methodological
500 approach used in this study for both Monod and Contois models is based on an effective
501 representation of concentrations and parameters at the mm- to cm-scale of measurements.
502 These effective concentrations and parameters conceptually integrate the smaller-scale
503 processes highlighted by other studies (Ebrahimi and Or, 2014; Portell et al., 2018; Tecon et
504 al., 2018). Such microscale processes should be addressed for further generalization beyond
505 the conditions of the soil experiments analyzed here. Despite its advantages, Contois models
506 have also a drawback with the fact that the modeled uptake efficiency of bacteria
507 approaches infinity for low densities, which does not correspond to any physical nor
508 biochemical process (Gleeson, 1994; Abrams, 2015). However, this side effect mostly affects
509 a negligible fraction of the bacteria and the substrate, as it was the case in the soil conditions
510 represented by the experiments.

511 Further work is required to confront the relevance of the Contois model to other soil
512 systems. To the best of our knowledge, ratio-dependent growth models such as the Contois
513 model have not yet been considered for the modeling of microbial degradation in soils.
514 However, the Contois growth equation is generally accepted to be more appropriate than
515 the Monod equation for modeling immobilized, heterogeneously distributed or mixed
516 microbial cultures (Arditi and Saiah, 1992; Harmand and Godon, 2007), all of which are
517 characteristics of soils. The regulation of individual activity by population density has
518 frequently been justified as a “crowding effect” associated with high population densities
519 leading to competition for substrate (Lobry and Harmand, 2006; Harmand and Godon, 2007;
520 Krichen et al., 2018). However, little is known about possible density regulation when
521 apparent microbial densities are low, as is observed in bulk soil (Raynaud and Nunan, 2014;
522 Kuzyakov and Blagodatskaya, 2015), although some studies have mentioned
523 ratio-dependence in highly-diluted environments such as aquifers (Hansen et al., 2017). As
524 discussed in section 4.1.1, the high maximum uptake efficiencies commonly observed for soil
525 bacteria adapted to oligotrophic environments are relevant to draw attention on the
526 potential significance of density control at low densities in oligotrophic soils, and thus
527 ratio-dependent models, among which the Contois model is a consistent choice.

528 ***4.3. Hypothetical relationship between bacterial traits and their spatial*** 529 ***strategies***

530 Density regulation might be at the origin of a relationship between bacterial oligotrophy,
531 their location in soil and their mobility strategy. Soil copiotroph bacteria have a maximum
532 uptake efficiency mostly between $100 \text{ l}\cdot\text{g}^{-1}\cdot\text{d}^{-1}$ (Button, 1991) and $800 \text{ l}\cdot\text{g}^{-1}\cdot\text{d}^{-1}$ (Daugherty and

533 Karel, 1994; Zelenev et al., 2005). For copiotrophs with maximum uptake efficiency values
534 below $288 \text{ l}\cdot\text{g}^{-1}\cdot\text{d}^{-1}$, bacterial dispersion was largely detrimental to their activity (**Fig. 4** blue
535 line, **Fig. 6**), in agreement with the results of Pagel et al. (2020), suggesting that copiotrophs
536 have more aggregated distributions than oligotrophs. The negligible mineralization even
537 without dispersion (**Fig. 3-A4**) also highlights the fact that copiotrophs are particularly
538 inefficient at degrading substrates that diffuse in the environment, as also evidenced by
539 Babey et al. (2017). To maintain significant activity, soil copiotrophs are likely to remain
540 immobile in the close surroundings of the substrate source or any immobile substrate, likely
541 attached to surfaces or embedded in EPS matrices. If not, they would be dispersed towards
542 more diluted area where their low maximum uptake efficiency would result in negligible
543 uptake. On the contrary, to survive and develop, soil oligotrophs should be able to easily
544 disperse and escape high competition areas. Given that soil is a poor and heterogeneous
545 environment, this dispersion would be essentially passive (Nunan et al., 2020), through
546 advective processes for example. We therefore suggest the existence of a theoretical
547 relationship between proximity to substrate sources (respectively remoteness), copiotrophy
548 (respectively oligotrophy) and attachment (respectively mobility).

549 **5. Conclusions**

550 Heterogeneous distributions of degraders and substrate in soils strongly control soil organic
551 matter degradation through their interactions with the bacterial activity. Taking 2,4-D as a
552 model organic solute substrate for soil bacteria, we investigated the coupled effects of
553 bacteria and substrate distributions on one side and bacterial traits on the other side on
554 substrate degradation. The analysis of published experiments with contrasted spreading

555 conditions of both bacteria and substrate reveals that, in addition to the distance of bacteria
556 from high substrate concentrations, mineralization is also surprisingly limited by the
557 bacterial density even under the low bacterial densities commonly observed in bulk soils.
558 Moreover, the impact of bacterial dispersion on solute substrate degradation can shift from
559 negative to positive depending on the bacterial maximum uptake efficiency. The activity of
560 soil oligotrophs may be mostly regulated by bacterial density rather than by substrate
561 dilution, echoing the population size paradox regularly observed. It follows that the
562 ratio-dependent Contois model might be more relevant to model bulk soil mineralization in
563 the heterogeneous conditions investigated than the substrate-dependent Monod model. To
564 predict the impact of spatial distributions on degradation in oligotrophic soil, and more
565 particularly the impact of bacterial dispersion, we suggest that bacterial densities might be
566 a more useful measurement than the volumes of soil devoid or occupied with bacteria. With
567 respect to the current lack of direct microscale data on microbial processes and distributions,
568 we propose some key perspectives on the bacterial kinetics and distributions.

569 **Acknowledgements**

570 This work was supported by the Agence Nationale de la Recherche through the project
571 “Soil μ -3D” [grant number ANR-15-CE01-0006] and was also partially supported by the SLAC
572 Floodplain Hydro-Biogeochemistry Science Focus Area (SFA), which is funded by the U.S.
573 Department of Energy (DOE) office of Biological and Environmental Research (BER), Climate
574 and Environmental Sciences Division, under DOE contract No. DE- AC02-76SF00515 to SLAC.
575 The authors thank Jérôme Harmand, Théodore Bouchez, Xavier Raynaud, Tanguy Le Borgne,

576 Claire Chenu and Holger Pagel for insightful discussions. The authors would also like to thank
577 the two anonymous referees and the editor for their constructive and valuable comments.

578 **Appendix A. Supplementary Data**

579 **References**

- 580 Abbott, A.J., Nelsestuen, G.L., 1988. The collisional limit: an important consideration for
581 membrane-associated enzymes and receptors. *The FASEB Journal* 2, 2858–2866.
582 <https://doi.org/10.1096/fasebj.2.13.2844615>
- 583 Abrams, P.A., 2015. Why ratio dependence is (still) a bad model of predation: Ratio-
584 dependent predation. *Biological Reviews* 90, 794–814.
585 <https://doi.org/10.1111/brv.12134>
- 586 Arditi, R., Saiah, H., 1992. Empirical evidence of the role of heterogeneity in ratio-
587 dependent consumption. *Ecology* 73, 1544–1551. <https://doi.org/10.2307/1940007>
- 588 Babey, T., Vieublé Gonod, L., Rapaport, A., Pinheiro, M., Garnier, P., de Dreuzy, J.-R., 2017.
589 Spatiotemporal simulations of 2,4-D pesticide degradation by microorganisms in 3D
590 soil-core experiments. *Ecological Modelling* 344, 48–61.
591 <https://doi.org/10.1016/j.ecolmodel.2016.11.006>
- 592 Bælum, J., Henriksen, T., Hansen, H.C.B., Jacobsen, C.S., 2006. Degradation of 4-chloro-2-
593 methylphenoxyacetic acid in top- and subsoil is quantitatively linked to the class III
594 *tfdA* gene. *Applied and Environmental Microbiology* 72, 1476–1486.
595 <https://doi.org/10.1128/AEM.72.2.1476-1486.2006>

- 596 Bælum, J., Nicolaisen, M.H., Holben, W.E., Strobel, B.W., Sørensen, J., Jacobsen, C.S., 2008.
597 Direct analysis of *tfdA* gene expression by indigenous bacteria in phenoxy acid
598 amended agricultural soil. *The ISME Journal* 2, 677–687.
599 <https://doi.org/10.1038/ismej.2008.21>
- 600 Balkwill, D.L., Leach, F.R., Wilson, J.T., McNabb, J.F., White, D.C., 1988. Equivalence of
601 microbial biomass measures based on membrane lipid and cell wall components,
602 adenosine triphosphate, and direct counts in subsurface aquifer sediments.
603 *Microbial Ecology* 16, 73–84. <https://doi.org/10.1007/BF02097406>
- 604 Boivin, A., Amellal, S., Schiavon, M., van Genuchten, M.Th., 2005. 2,4-
605 dichlorophenoxyacetic acid (2,4-D) sorption and degradation dynamics in three
606 agricultural soils. *Environmental Pollution* 138, 92–99.
607 <https://doi.org/10.1016/j.envpol.2005.02.016>
- 608 Breitenbeck, G.A., Yang, H., Dunigan, E.P., 1988. Water-facilitated dispersal of inoculant
609 *Bradyrhizobium japonicum* in soils. *Biology and Fertility of Soils* 7, 58–62.
610 <https://doi.org/10.1007/BF00260733>
- 611 Bünemann, E.K., Bongiorno, G., Bai, Z., Creamer, R.E., De Deyn, G., de Goede, R., Fleskens,
612 L., Geissen, V., Kuyper, T.W., Mäder, P., Pulleman, M., Sukkel, W., van Groenigen,
613 J.W., Brussaard, L., 2018. Soil quality – A critical review. *Soil Biology and*
614 *Biochemistry* 120, 105–125. <https://doi.org/10.1016/j.soilbio.2018.01.030>
- 615 Button, D.K., 1978. On the theory of control of microbial growth kinetics by limiting
616 nutrient concentrations. *Deep Sea Research* 25, 1163–1177.
617 [https://doi.org/10.1016/0146-6291\(78\)90011-5](https://doi.org/10.1016/0146-6291(78)90011-5)

- 618 Button, D.K., 1983. Differences between the kinetics of nutrient uptake by micro-
619 organisms, growth and enzyme kinetics. *Trends in Biochemical Sciences* 8, 121–124.
620 [https://doi.org/10.1016/0968-0004\(83\)90232-3](https://doi.org/10.1016/0968-0004(83)90232-3)
- 621 Button, D.K., 1991. Biochemical basis for whole-cell uptake kinetics: specific affinity,
622 oligotrophic capacity, and the meaning of the michaelis constant. *Applied and*
623 *Environmental Microbiology* 57, 2033–2038.
- 624 Button, D.K., 1993. Nutrient-limited microbial growth kinetics: overview and recent
625 advances. *Antonie van Leeuwenhoek* 63, 225–235.
626 <https://doi.org/10.1007/BF00871220>
- 627 Carrayrou, J., Mosé, R., Behra, P., 2004. Operator-splitting procedures for reactive
628 transport and comparison of mass balance errors. *Journal of Contaminant*
629 *Hydrology* 68, 239–268. doi:10.1016/S0169-7722(03)00141-4
- 630 Cheyns, K., Mertens, J., Diels, J., Smolders, E., Springael, D., 2010. Monod kinetics rather
631 than a first-order degradation model explains atrazine fate in soil mini-columns:
632 Implications for pesticide fate modelling. *Environmental Pollution* 158, 1405–1411.
633 <https://doi.org/10.1016/j.envpol.2009.12.041>
- 634 Contois, D.E., 1959. Kinetics of bacterial growth: relationship between population density
635 and specific growth rate of continuous cultures. *Journal of General Microbiology* 21,
636 40–50. <https://doi.org/10.1099/00221287-21-1-40>
- 637 Daugherty, D.D., Karel, S.F., 1994. Degradation of 2,4-dichlorophenoxyacetic acid by
638 *Pseudomonas cepacia* DBOI(pRO101) in a dual-substrate chemostat. *Applied and*
639 *Environmental Microbiology* 60, 3261–3267.

- 640 Dechesne, A., Owsianiak, M., Bazire, A., Grundmann, G.L., Binning, P.J., Smets, B.F., 2010.
641 Biodegradation in a partially saturated sand matrix: compounding effects of water
642 content, bacterial spatial distribution, and motility. *Environmental Science &*
643 *Technology* 44, 2386–2392. <https://doi.org/10.1021/es902760y>
- 644 Dechesne, A., Badawi, N., Aamand, J., Smets, B.F., 2014. Fine scale spatial variability of
645 microbial pesticide degradation in soil: scales, controlling factors, and implications.
646 *Frontiers in Microbiology* 5, 667. <https://doi.org/10.3389/fmicb.2014.00667>
- 647 Desmond-Le Quémener, E., Bouchez, T., 2014. A thermodynamic theory of microbial
648 growth. *The ISME Journal* 8, 1747–1751. doi:10.1038/ismej.2014.7
- 649 Don, R.H., Weightman, A.J., 1985. Transposon mutagenesis and cloning analysis of the
650 pathways for degradation of 2,4-dichlorophenoxyacetic acid and 3-chlorobenzoate
651 in *Alcaligenes eutrophus* JMP134(pJP4). *Journal of Bacteriology* 161, 85–90.
- 652 Ebrahimi, A.N., Or, D., 2014. Microbial dispersal in unsaturated porous media:
653 Characteristics of motile bacterial cell motions in unsaturated angular pore
654 networks. *Water Resources Research* 50, 7406–7429. doi:10.1002/2014WR015897
- 655 Fierer, N., Bradford, M.A., Jackson, R.B., 2007. Toward an ecological classification of soil
656 bacteria. *Ecology* 88, 1354–1364. <https://doi.org/10.1890/05-1839>
- 657 Gleeson, S.K., 1994. Density dependence is better than ratio dependence. *Ecology* 75,
658 1834–1835. <https://doi.org/10.2307/1939642>
- 659 Gözdereliler, E., Boon, N., Aamand, J., De Roy, K., Granitsiotis, M.S., Albrechtsen, H.J.,
660 Sørensen, S.R., 2012. Comparing metabolic functionality, community structure and
661 dynamics of herbicide-degrading communities. *Applied and Environmental*
662 *Microbiology*.

- 663 Haegeman, B., Rapaport, A., 2008. How flocculation can explain coexistence in the
664 chemostat. *Journal of Biological Dynamics* 2, 1–13.
665 <https://doi.org/10.1080/17513750801942537>
- 666 Hammond, E.C., 1938. Biological effects of population density in lower organisms. *The*
667 *Quarterly Review of Biology* 13, 421–438. <http://www.jstor.org/stable/2808555>
- 668 Hansen, S.K., Pandey, S., Karra, S., Vesselinov, V.V., 2017. CHROTRAN: A mathematical and
669 computational model for in situ heavy metal remediation in heterogeneous
670 aquifers. *ArXiv:1703.01381 [q-Bio]*.
- 671 Harmand, J., Godon, J.J., 2007. Density-dependent kinetics models for a simple description
672 of complex phenomena in macroscopic mass-balance modeling of bioreactors.
673 *Ecological Modelling* 200, 393–402.
674 <https://doi.org/10.1016/j.ecolmodel.2006.08.012>
- 675 Healey, F.P., 1980. Slope of the Monod equation as an indicator of advantage in nutrient
676 competition. *Microbial Ecology* 5, 281–286. <http://www.jstor.org/stable/4250586>
- 677 Holden, P.A., Firestone, M.K., 1997. Soil microorganisms in soil cleanup: How can we
678 improve our understanding? *Journal of Environment Quality* 26, 32–40.
679 <https://doi.org/10.2134/jeq1997.00472425002600010006x>
- 680 Holden, P.A., Hunt, J.R., Firestone, M.K., 1997. Toluene diffusion and reaction in
681 unsaturated *Pseudomonas putida* biofilms. *BIOTECHNOLOGY AND*
682 *BIOENGINEERING* 56, 15.
- 683 Iserles, A., 2009. *A first course in the numerical analysis of differential equations*,
684 Cambridge University Press. ed.

- 685 Juyal, A., Otten, W., Falconer, R., Hapca, S., Schmidt, H., Baveye, P.C., Eickhorst, T., 2019.
686 Combination of techniques to quantify the distribution of bacteria in their soil
687 microhabitats at different spatial scales. *Geoderma* 334, 165–174.
688 <https://doi.org/10.1016/j.geoderma.2018.07.031>
- 689 Kemmitt, S.J., Lanyon, C.V., Waite, I.S., Wen, Q., Addiscott, T.M., Bird, N.R.A., O'Donnell,
690 A.G., Brookes, P.C., 2008. Mineralization of native soil organic matter is not
691 regulated by the size, activity or composition of the soil microbial biomass—a new
692 perspective. *Soil Biology and Biochemistry* 40, 61–73.
693 <https://doi.org/10.1016/j.soilbio.2007.06.021>
- 694 Koch, A.L., 1971. The adaptive responses of *Escherichia coli* to a feast and famine existence,
695 in: *Advances in Microbial Physiology*. Elsevier, pp. 147–217.
696 [https://doi.org/10.1016/S0065-2911\(08\)60069-7](https://doi.org/10.1016/S0065-2911(08)60069-7)
- 697 König, S., Vogel, H.-J., Harms, H., Worrlich, A., 2020. Physical, chemical and biological effects
698 on soil bacterial dynamics in microscale models. *Frontiers in Ecology and Evolution*
699 8, 53. <https://doi.org/10.3389/fevo.2020.00053>
- 700 Krichen, E., Harmand, J., Torrijos, M., Godon, J.J., Bernet, N., Rapaport, A., 2018. High
701 biomass density promotes density-dependent microbial growth rate. *Biochemical*
702 *Engineering Journal* 130, 66–75. <https://doi.org/10.1016/j.bej.2017.11.017>
- 703 Kuzyakov, Y., Blagodatskaya, E., 2015. Microbial hotspots and hot moments in soil: Concept
704 & review. *Soil Biology and Biochemistry* 83, 184–199.
705 <https://doi.org/10.1016/j.soilbio.2015.01.025>
- 706 Lagneau, V., van der Lee, J., 2010. Operator-splitting-based reactive transport models in
707 strong feedback of porosity change: The contribution of analytical solutions for

- 708 accuracy validation and estimator improvement. *Journal of Contaminant Hydrology*
709 112, 118–129. doi:10.1016/j.jconhyd.2009.11.005
- 710 Lobry, C., Harmand, J., 2006. A new hypothesis to explain the coexistence of n species in
711 the presence of a single resource. *Comptes Rendus Biologies* 329, 40–46.
712 <https://doi.org/10.1016/j.crv.2005.10.004>
- 713 Lobry, J.R., Flandrois, J.P., Carret, G., Pave, A., 1992. Monod's bacterial growth model
714 revisited. *Bulletin of Mathematical Biology* 54, 117–122.
715 <https://doi.org/10.1007/BF02458623>
- 716 Madsen, E.L., Alexander, M., 1982. Transport of Rhizobium and Pseudomonas through Soil.
717 *Soil Science Society of America Journal* 46, 557–560.
718 <https://doi.org/10.2136/sssaj1982.03615995004600030023x>
- 719 Monod, J., 1949. The growth of bacterial cultures. *Annual Review of Microbiology* 3, 371–
720 394. <https://doi.org/10.1146/annurev.mi.03.100149.002103>
- 721 Nelson, M.I., Holder, A., 2009. A fundamental analysis of continuous flow bioreactor
722 models governed by Contois kinetics. II. Reactor cascades. *Chemical Engineering*
723 *Journal* 149, 406–416. <https://doi.org/10.1016/j.cej.2009.01.028>
- 724 Nunan, N., Young, I.M., Crawford, J.W., Ritz, K., 2007. Bacterial interactions at the
725 microscale - Linking habitat to function in soil, in: Franklin, R., Mills, A. (Eds.), *The*
726 *Spatial Distribution of Microbes in the Environment*. Springer, Dordrecht, pp. 61–85.
- 727 Nunan, N., Schmidt, H., Raynaud, X., 2020. The ecology of heterogeneity: soil bacterial
728 communities and C dynamics. *Philosophical Transactions of the Royal Society B:*
729 *Biological Sciences* 375, 20190249. <https://doi.org/10.1098/rstb.2019.0249>

- 730 Ohta, H., Taniguchi, S., 1988. Growth characteristics of the soil oligotrophic bacterium:
731 *Agromonas oligotrophica* JCM 1494 on diluted nutrient broth. *The Journal of*
732 *General and Applied Microbiology* 34, 349–353.
733 <https://doi.org/10.2323/jgam.34.349>
- 734 Or, D., Smets, B.F., Wraith, J.M., Dechesne, A., Friedman, S.P., 2007. Physical constraints
735 affecting bacterial habitats and activity in unsaturated porous media – a review.
736 *Advances in Water Resources* 30, 1505–1527. doi:10.1016/j.advwatres.2006.05.025
- 737 Pagel, H., Kriesche, B., Uksa, M., Poll, C., Kandeler, E., Schmidt, V., Streck, T., 2020. Spatial
738 control of carbon dynamics in soil by microbial decomposer communities. *Frontiers*
739 *in Environmental Science* 8, 2. <https://doi.org/10.3389/fenvs.2020.00002>
- 740 Pallud, C., Dechesne, A., Gaudet, J.P., Debouzie, D., Grundmann, G.L., 2004. Modification of
741 spatial distribution of 2,4-dichlorophenoxyacetic acid degrader microhabitats during
742 growth in soil columns. *Applied and Environmental Microbiology* 70, 2709–2716.
743 <https://doi.org/10.1128/AEM.70.5.2709-2716.2004>
- 744 Patarinska, T., Dochain, D., Agathos, S.N., Ganovski, L., 2000. Modelling of continuous
745 microbial cultivation taking into account the memory effects. *Bioprocess*
746 *Engineering* 22, 517–527. <https://doi.org/10.1007/s004499900095>
- 747 Pfeiffer, T., Schuster, S., Bonhoeffer, S., 2001. Cooperation and Competition in the
748 Evolution of ATP-Producing Pathways 292, 5.
- 749 Pieper, D.H., Reineke, W., Engesser, K.-H., Knackmuss, H.-J., 1988. Metabolism of 2,4-
750 dichlorophenoxyacetic acid, 4-chloro-2-methylphenoxyacetic acid and 2-
751 methylphenoxyacetic acid by *Alcaligenes eutrophus* JMP 134. *Archives of*
752 *Microbiology* 150, 95–102. <https://doi.org/10.1007/BF00409724>

- 753 Pinheiro, M., Garnier, P., Beguet, J., Martin Laurent, F., Vieublé Gonod, L., 2015. The
754 millimetre-scale distribution of 2,4-D and its degraders drives the fate of 2,4-D at
755 the soil core scale. *Soil Biology and Biochemistry* 88, 90–100.
756 <https://doi.org/10.1016/j.soilbio.2015.05.008>
- 757 Pinheiro, M., Pagel, H., Poll, C., Ditterich, F., Garnier, P., Streck, T., Kandeler, E., Vieublé
758 Gonod, L., 2018. Water flow drives small scale biogeography of pesticides and
759 bacterial pesticide degraders - A microcosm study using 2,4-D as a model
760 compound. *Soil Biology and Biochemistry* 127, 137–147.
761 <https://doi.org/10.1016/j.soilbio.2018.09.024>
- 762 Poll, C., Ingwersen, J., Stemmer, M., Gerzabek, M.H., Kandeler, E., 2006. Mechanisms of
763 solute transport affect small-scale abundance and function of soil microorganisms
764 in the detritosphere. *European Journal of Soil Science* 57, 583–595.
765 <https://doi.org/10.1111/j.1365-2389.2006.00835.x>
- 766 Portell, X., Pot, V., Garnier, P., Otten, W., Baveye, P.C., 2018. Microscale Heterogeneity of
767 the Spatial Distribution of Organic Matter Can Promote Bacterial Biodiversity in
768 Soils: Insights From Computer Simulations. *Frontiers in Microbiology* 9, 1583.
769 [doi:10.3389/fmicb.2018.01583](https://doi.org/10.3389/fmicb.2018.01583)
- 770 Rapaport, A., 2018. Properties of the chemostat model with aggregated biomass. *European*
771 *Journal of Applied Mathematics* 29, 972–990.
772 <https://doi.org/10.1017/S0956792518000141>
- 773 Raynaud, X., Nunan, N., 2014. Spatial Ecology of Bacteria at the Microscale in Soil. *PLoS*
774 *ONE* 9, e87217. <https://doi.org/10.1371/journal.pone.0087217>

- 775 Read, C.P., 1951. The “Crowding Effect” in Tapeworm Infections. *The Journal of*
776 *Parasitology* 37, 174–178. <https://doi.org/10.2307/3273449>
- 777 Roller, B.R., Schmidt, T.M., 2015. The physiology and ecological implications of efficient
778 growth. *The ISME Journal* 9, 1481–1487. <https://doi.org/10.1038/ismej.2014.235>
- 779 Shampine, L.F., Reichelt, M.W., 1997. The MATLAB ODE Suite. *SIAM Journal on Scientific*
780 *Computing* 18, 1–22. <https://doi.org/10.1137/S1064827594276424>
- 781 Sibly, R.M., Hone, J., 2002. Population growth rate and its determinants: an overview.
782 *Philosophical Transactions of the Royal Society of London. Series B: Biological*
783 *Sciences* 357, 1153–1170. <https://doi.org/10.1098/rstb.2002.1117>
- 784 Sinton, G.L., Fan, L.T., Erickson, L.E., Lee, S.M., 1986. Biodegradation of 2,4-D and related
785 xenobiotic compounds. *Enzyme and Microbial Technology* 8, 395–403.
786 [https://doi.org/10.1016/0141-0229\(86\)90145-6](https://doi.org/10.1016/0141-0229(86)90145-6)
- 787 Smoluchowski, M. v, 1918. Versuch einer mathematischen Theorie der Koagulationskinetik
788 kolloider Lösungen. *Zeitschrift für Physikalische Chemie* 92U, 129–168.
789 <https://doi.org/10.1515/zpch-1918-9209>
- 790 Stana, R.L., 2020. Diffusive transport: theory and application (Doctor of Philosophy thesis).
791 University of Leeds, UK.
- 792 Tecon, R., Or, D., 2017. Biophysical processes supporting the diversity of microbial life in
793 soil. *FEMS Microbiology Reviews* 41, 599–623.
794 <https://doi.org/10.1093/femsre/fux039>
- 795 Tecon, R., Ebrahimi, A., Kleyer, H., Erev Levi, S., Or, D., 2018. Cell-to-cell bacterial
796 interactions promoted by drier conditions on soil surfaces. *Proceedings of the*
797 *National Academy of Sciences* 115, 9791–9796. doi:10.1073/pnas.1808274115

- 798 Tuxen, N., de Liphay, J.R., Albrechtsen, H.-J., Aamand, J., Bjerg, P.L., 2002. Effect of
799 exposure history on microbial herbicide degradation in an aerobic aquifer affected
800 by a point source. *Environmental Science & Technology* 36, 2205–2212.
801 <https://doi.org/10.1021/es0113549>
- 802 Ugalde-Salas, P., Desmond-Le Quémener, E., Harmand, J., Rapaport, A., Bouchez, T., 2020.
803 Insights from Microbial Transition State Theory on Monod’s Affinity Constant.
804 *Scientific Reports* 10, 5323. doi:10.1038/s41598-020-62213-6
- 805 Vieublé Gonod, L., Chenu, C., Soulas, G., 2003. Spatial variability of 2,4-
806 dichlorophenoxyacetic acid (2,4-D) mineralisation potential at a millimetre scale in
807 soil. *Soil Biology and Biochemistry* 35, 373–382. [https://doi.org/10.1016/S0038-](https://doi.org/10.1016/S0038-0717(02)00287-0)
808 [0717\(02\)00287-0](https://doi.org/10.1016/S0038-0717(02)00287-0)
- 809 Young, I.M., Crawford, J.W., Nunan, N., Otten, W., Spiers, A., 2008. Chapter 4 Microbial
810 distribution in soils, in: *Advances in Agronomy*. Elsevier, pp. 81–121.
811 [https://doi.org/10.1016/S0065-2113\(08\)00604-4](https://doi.org/10.1016/S0065-2113(08)00604-4)
- 812 Zelenev, V.V., van Bruggen, A.H.C., Semenov, A.M., 2005. Modeling wave-like dynamics of
813 oligotrophic and copiotrophic bacteria along wheat roots in response to nutrient
814 input from a growing root tip. *Ecological Modelling* 188, 404–417.
815 <https://doi.org/10.1016/j.ecolmodel.2005.01.046>
816

817 **Tables**818 **Table 1.**

819 Values and range of values of the reactive transport model. The effective dispersion
 820 coefficient d_{disp} applies only to heterogeneous percolation experiments. $B(t=0)$ is the initial
 821 density of bacteria in the natural cubes. It is considered 1.6 times smaller in the percolation
 822 experiments than in the hydrostatic experiments according to the initial experimental
 823 measurements.

Parameter description		Symbol	Unit	Fixed values and admissible ranges for screening
initial substrate concentration	hydrostatic experiments	$S(t=0)$	$\mu\text{g}\cdot\text{g}^{-1}$ (mass of substrate carbon per mass of dry soil)	0.825 ^b
	percolation experiments		$\mu\text{g}\cdot\text{g}^{-1}$	6.52 ^b
reversible adsorption coefficient		k_{SA}	d^{-1}	0.09207
reversible desorption coefficient		k_{AS}	d^{-1}	4.361
irreversible adsorption coefficient		k_C	d^{-1}	0.01296
uptake yield		y	-	0.5206
maximum specific uptake rate		$(1/y)\cdot\mu_{max}$	d^{-1}	[0.0190 – 19.5]
uptake efficiency at the lowest substrate concentration		$(1/y)\cdot\mu_{max}/\kappa^a$ where κ is κ_M or $B(t=0)\cdot\kappa_C$	$\text{g}\cdot\mu\text{g}^{-1}\cdot\text{d}^{-1}$ (mass of dry soil per mass of bacterial carbon per unit of time)	[0.0152 – 159] ^c
accommodation rate		α	d^{-1}	[0.00934 – 934]
initial degrader	hydrostatic experiments	$B(t=0)$	$\mu\text{g}\cdot\text{g}^{-1}$ (mass of bacterial carbon per mass of dry soil)	[0.0161 – 1.61] ^d

population density	percolation experiments	$B(t=0)$	$\mu\text{g}\cdot\text{g}^{-1}$	$[0.0101 - 1.01]^d$
mortality rate		m_t	d^{-1}	0.0602
biomass recycling yield		χ	-	0.6010
effective diffusion coefficient		d_{diff}	$\text{m}^2\cdot\text{d}^{-1}$	$1 \cdot 10^{-5}^e$
effective dispersion coefficient		d_{disp}	$\text{m}^2\cdot\text{d}^{-1}$	$[0 - \infty]$
leaching rates (days 0; 3; 6)	homogeneous experiments heterogeneous experiments	ν	-	0.108; 0.226; 0.180 0.107; 0.223; 0.178

824 ^a The half-saturation constant κ corresponds to κ_M for the Monod-based model and $B(t=0)\cdot\kappa_C$
 825 for the Contois-based model (where $B(t=0)$ is the value from the hydrostatic experiments).

826 ^b The initial substrate concentration $S(t=0)$ is set equal to the ¹⁴C-2,4-D concentration
 827 amended in the experiments.

828 ^c The values of $(1/y)\cdot\mu_{max}/\kappa$ correspond to ranges of $[1.65 - 1.73 \cdot 10^4]$ $\text{l}\cdot\text{g}^{-1}\cdot\text{d}^{-1}$ (volume of
 829 water per mass of bacteria per unit of time)

830 ^d The values of $B(t=0)$ correspond respectively to ranges of $[1.48 \cdot 10^{-4} - 1.48 \cdot 10^{-2}]$ $\text{g}\cdot\text{l}^{-1}$ (mass
 831 of bacteria per volume of water) for the hydrostatic experiments and $[9.24 \cdot 10^{-5} - 9.24$
 832 $\cdot 10^{-3}]$ $\text{g}\cdot\text{l}^{-1}$ for the percolation experiments.

833 ^e The value of d_{diff} has been calibrated on a $3 \times 6 \times 6$ grid in similar conditions (Babey et al.,
 834 2017).

835

836 **Table 2.**

837 Parameters for the Monod-based model calibrated by the screening approach (section 2.2)
 838 on the hydrostatic experiments only (Babey et al., 2017) and on both hydrostatic and
 839 percolation experiments, and for the Contois-based model calibrated on both hydrostatic
 840 and percolation experiments, as described in section 2.4

Parameter symbol	Unit	Monod model calibration		Contois model calibration
		on the sole hydrostatic experiments	on both hydrostatic & percolation experiments	on both hydrostatic & percolation experiments
$(1/y) \cdot \mu_{max}$	d^{-1}	1.22	9.73	4.86
$(1/y) \cdot \mu_{max}/\kappa^a$	$g \cdot \mu g^{-1} \cdot d^{-1}$ (mass of dry soil per mass of bacterial carbon per unit of time)	2.65 ^b	26.5 ^b	2.65 ^b
α	d^{-1}	$9.341 \cdot 10^{-1}$	$9.34 \cdot 10^{-2}$	$9.34 \cdot 10^{-2}$
$B(t=0)$	hydrostatic experiments $\mu g \cdot g^{-1}$ (mass of bacterial carbon per mass of dry soil)	$1.61 \cdot 10^{-1}$	$3.23 \cdot 10^{-2}$	$3.76 \cdot 10^{-1}$
	percolation experiments $\mu g \cdot g^{-1}$	$1.01 \cdot 10^{-1}$	$2.01 \cdot 10^{-2}$	$2.34 \cdot 10^{-1}$
d_{disp}	$m^2 \cdot d^{-1}$	0 ^c	$1.78 \cdot 10^{-4}$ ^c	10^{-5} ^c
J_{1234}	-	0.079	0.032	0.022

841 ^a The half-saturation constant κ corresponds to κ_M for the Monod-based model and
 842 $B(t=0) \cdot \kappa_C$ for the Contois-based model (where $B(t=0)$ is the value from the hydrostatic
 843 experiments).

844 ^b Values of $(1/y) \cdot \mu_{max}/\kappa$ correspond respectively to $2.89 \cdot 10^2$, $2.89 \cdot 10^3$ and $2.89 \cdot 10^2$ $l \cdot g^{-1} \cdot d^{-1}$
 845 (volume of water per mass of bacteria per unit of time).

846 ^cThe corresponding spreading values induced by the hydrodynamic dispersion
847 (root-mean-square displacements) for each percolation events are respectively 0, 3.8 and
848 0.91 mm, to be compared to the 25 mm radius of the soil column.

Journal Pre-proof

1 **Figure captions**

2 **Fig. 1.** Model experimental design, geometry and initial distributions **(A)** based on previously
 3 performed experiments in hydrostatic (Pineiro et al., 2015) and percolation (Pineiro et al.,
 4 2018) conditions. The red and green arrows refer respectively to the 2,4-D and degrader
 5 modeled displacements. **(B)** Experimental cumulated production of CO₂ (adapted from
 6 Pineiro et al. (2018, 2015), permission for reproduction granted by Elsevier).

7

8 **Fig. 2.** Graphical representation of the biochemical model and carbon fluxes identified by the
 9 arrows. Under low substrate concentrations S , the specific uptake rate $(1/y)\cdot\mu$ becomes
 10 equal to $S\cdot(1/y)\cdot\mu_{max}/K_M$, where $(1/y)\cdot\mu_{max}/K_M$ is referred to as the “maximum uptake
 11 efficiency”.

12

13 **Fig. 3.** Mineralization dynamics predicted with the Monod-based model calibrated on the
 14 hydrostatic experiment only **(A)** and on both hydrostatic and percolation experiments **(B)**.
 15 The related experimental setups are indicated in the top right corner of each graph. The
 16 agreement between experiments and model is indicated by the value of discrepancy J
 17 displayed at the bottom and can be visually assessed by the proximity between the black line
 18 and the dots representing respectively the model results and experimental data. The red line
 19 refers to the carbon mass of substrate remaining in the soil core. In the percolation
 20 experiments **(A3,4 and B3,4)**, around 51% of the initial mass of ¹⁴C was lost through leaching
 21 at each percolation events ($t = 0, 3$ and 6 days, blue arrows). The carbon balance among the

22 different pools is detailed in **Fig. S11**. Note that the reversible sorption eventually accounted
23 for less than 2% of the initial carbon mass and therefore did not significantly alter the results.

24

25 **Fig. 4.** Influence of the dispersion coefficient d_{disp} on mineralization predicted at day 24
26 $m_{CO_2}(t=24)$ for the biological parameter set calibrated on the sole hydrostatic experiments
27 (**A**, thick red line) and on both hydrostatic and percolation experiments (**B**, thick blue line).
28 Note that for the model calibrated on both hydrostatic and percolation experiments, the
29 value of d_{disp} leading to the highest final mineralization ($d_{disp} = 1.78 \cdot 10^{-4} \text{ m}^2 \cdot \text{d}^{-1}$, thick blue
30 line) is also equal to its calibrated value leading to the best adequacy with mineralization
31 kinetics (**Table 2**). Note that the optimal dispersion value remains the same when
32 representing the remaining dissolved substrate instead of the mineralization (**Fig. S13**).

33

34 **Fig. 5.** Predicted substrate and bacterial spatial concentration profiles after 6 days of
35 diffusion and dispersion in the conditions of heterogeneous percolation experiment, in
36 which bacteria and substrate are initially located exclusively in the central cube (between 0
37 and 3 mm). Results are simulated on a $9 \times 18 \times 18$ grid obtained by subdividing the $3 \times 6 \times 6$
38 grid used for the screenings. The results are represented for the parameter set calibrated
39 using only the sole hydrostatic experiment, either with a moderate dispersion
40 ($d_{disp} = 1.78 \cdot 10^{-4} \text{ m}^2 \cdot \text{d}^{-1}$) (**A**) or with the calibrated dispersion (no dispersion) (**B**), and for the
41 biological parameter set calibrated on both hydrostatic and percolation experiments, either
42 without dispersion (**C**) or with the calibrated dispersion ($d_{disp} = 1.78 \cdot 10^{-4} \text{ m}^2 \cdot \text{d}^{-1}$) (**D**). On one
43 hand, bacteria are exposed to smaller substrate concentrations if they are far from the

44 source (right part of the substrate concentration profiles). On the other hand, bacteria
45 undergo competition if they are too close from each other (left part of the substrate
46 concentration profiles). In (C), the bacteria aggregated below d consume the substrate faster
47 than it is replenished by backward diffusion and dispersion. The total number of bacteria
48 within the whole soil column at day 6 is similar in (A), (B), (C) and (D), respectively equal to
49 $6.0 \cdot 10^5$, $9.5 \cdot 10^5$, $11.5 \cdot 10^5$ and $11.3 \cdot 10^5$. The final mineralization at day 24 is however strongly
50 different between scenario, reaching respectively 3.2%, 5.3%, 9.1% and 24.7% of the initial
51 mass of ^{14}C .

52

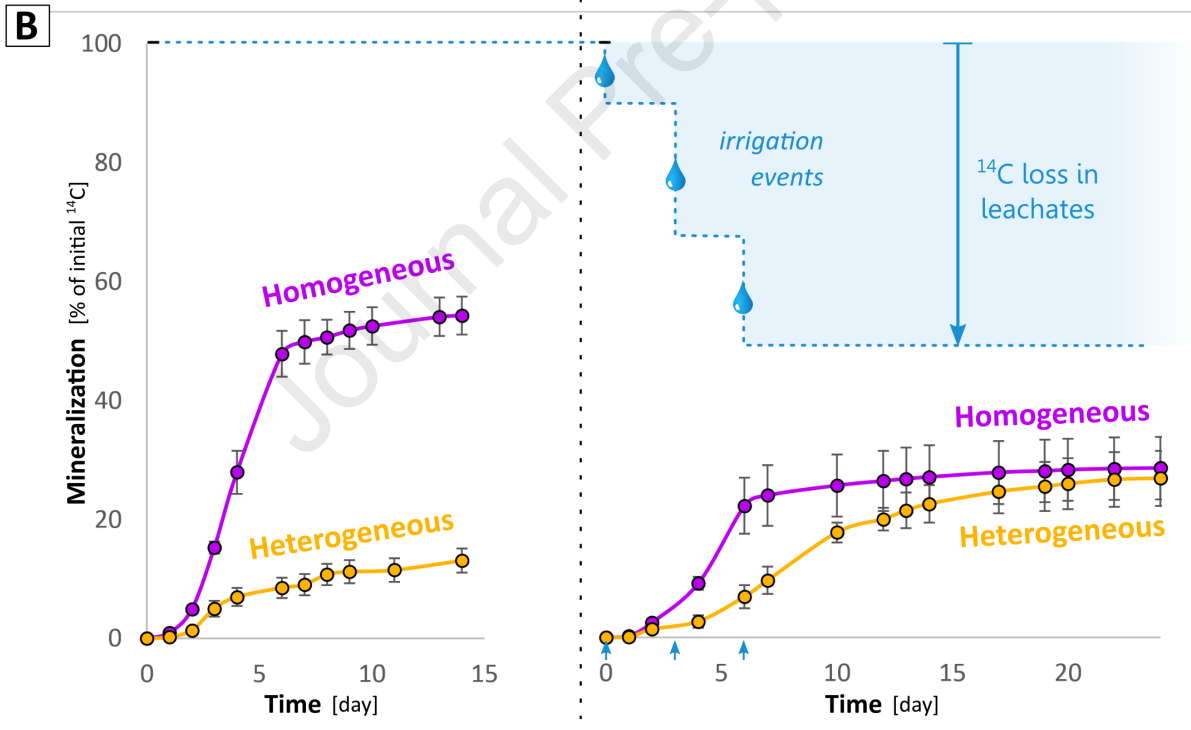
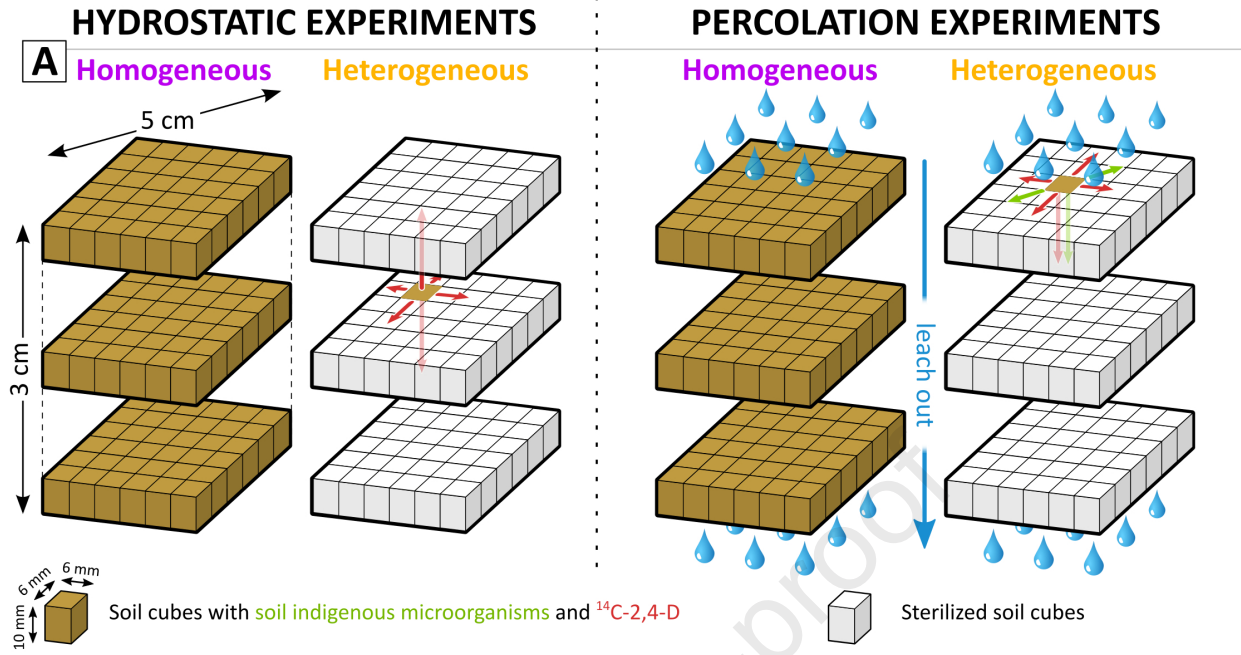
53 **Fig. 6.** Dispersion coefficient giving the highest predicted mineralization at day 24 as a
54 function of maximum uptake efficiency, all other parameters equal to those of the model
55 calibrated on both hydrostatic and percolation experiments.

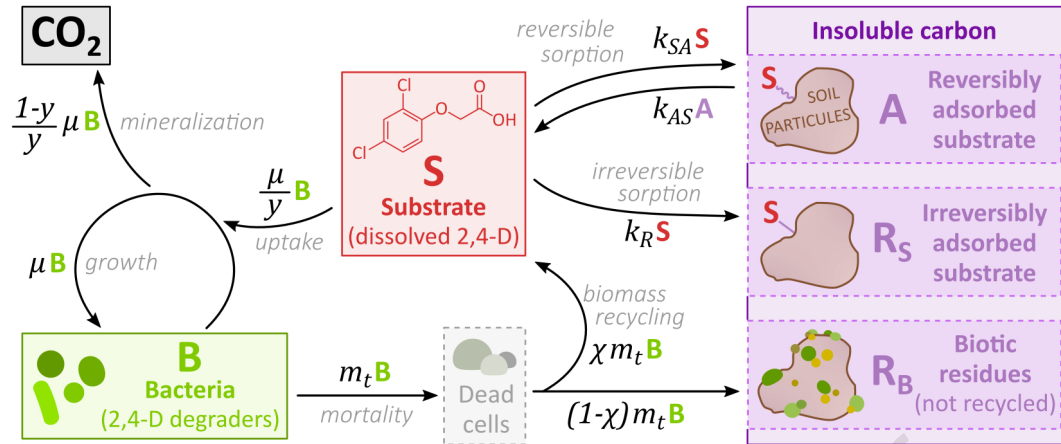
56

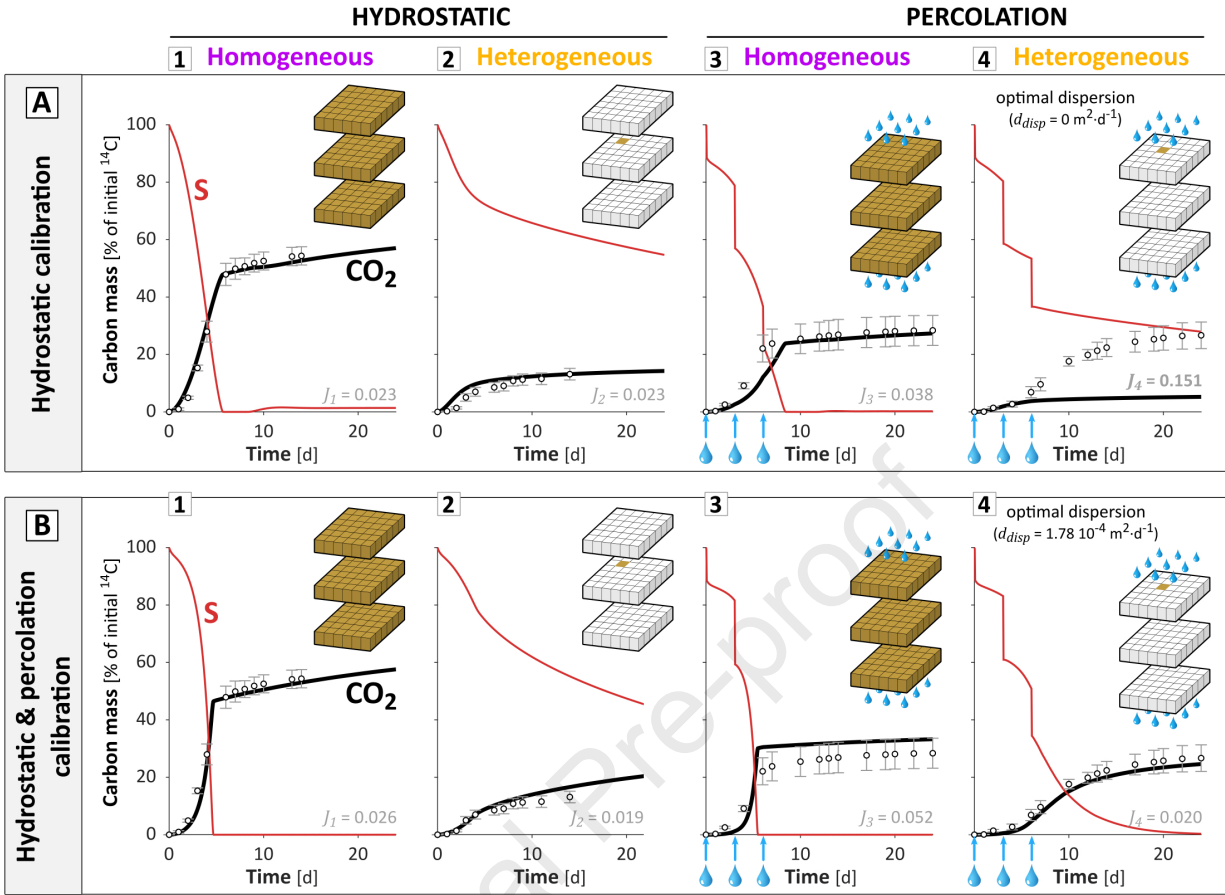
57 **Fig. 7.** Mineralization dynamics predicted with the Contois-based model calibrated on both
58 hydrostatic and percolation experiments. For representation and legend, see **Fig. 3**. The
59 carbon balance among the different pools is detailed in **Fig. S11**.

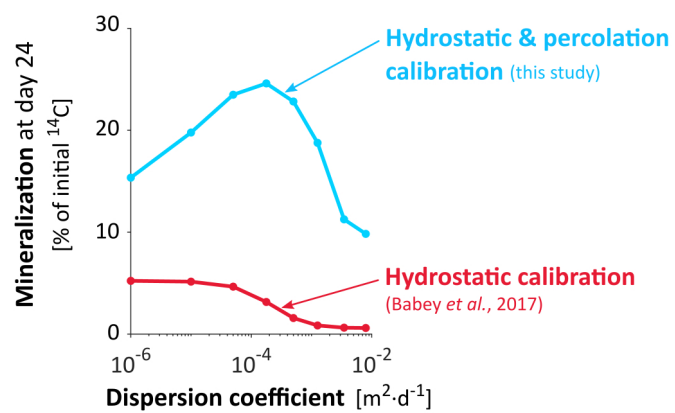
60

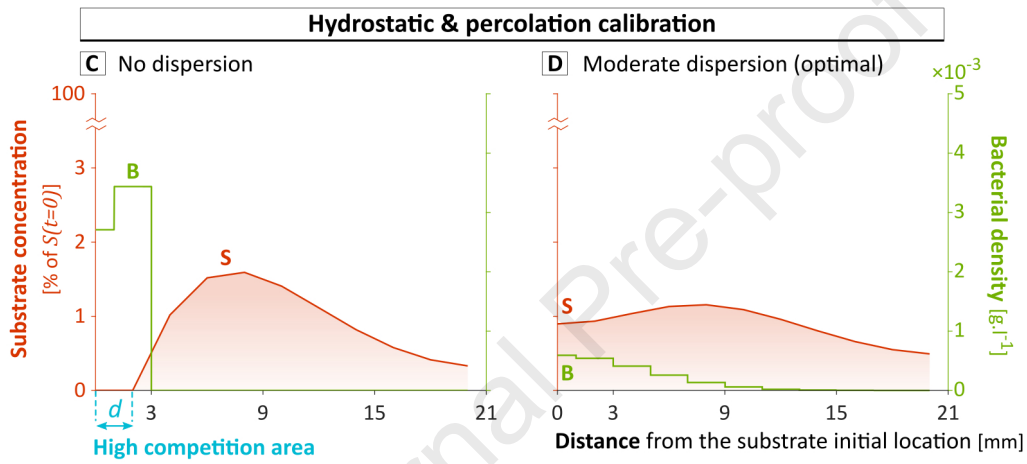
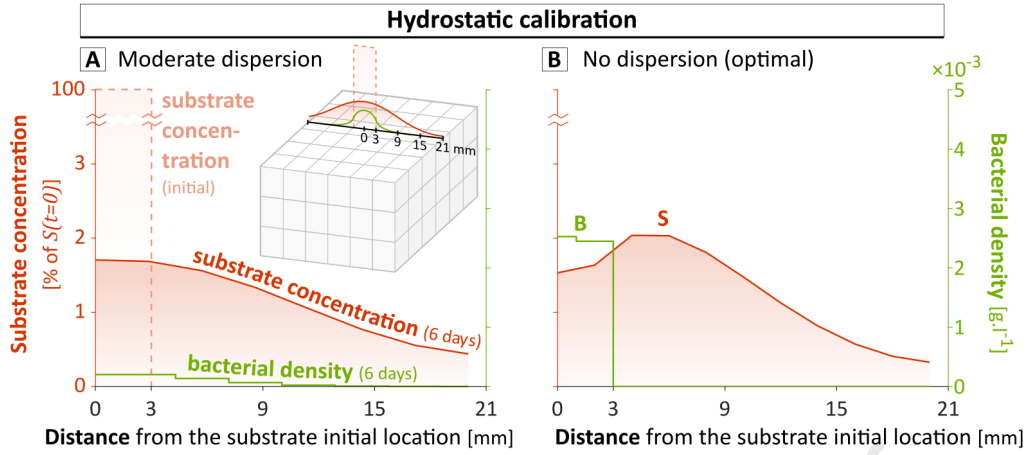
61 **Fig. 8.** Influence of the dispersion coefficient on mineralization at day 24 for the
62 Contois-based models calibrated on the sole hydrostatic experiments (thick red line) and on
63 both hydrostatic and percolation experiments (thick blue line). For representation and
64 legend, see **Fig. 4**.

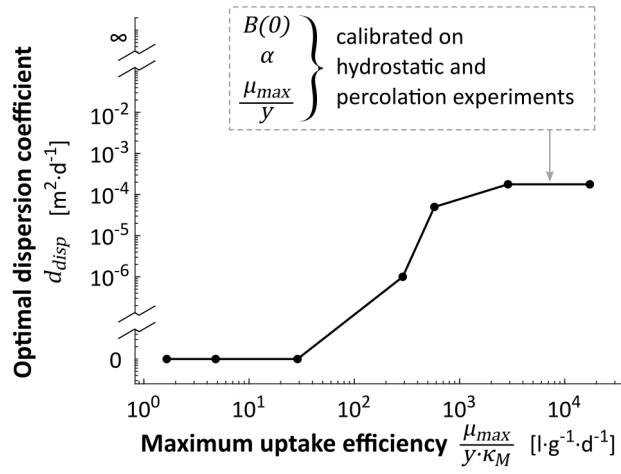


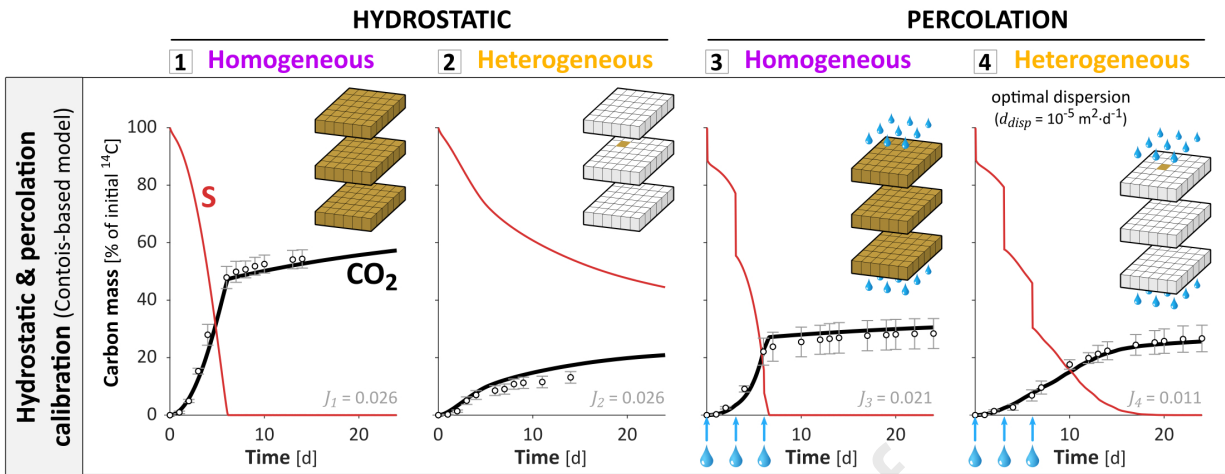


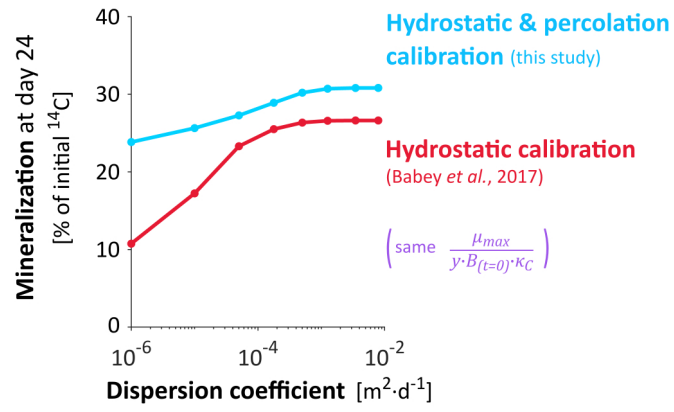


Monod-based model







Contois-based model

Journal Pre-proof

1 **Highlights**

- 2 - The impact of spatial distributions on decomposition depends on bacterial traits
- 3 - Decomposition can be reduced by competition between bacteria even at low densities
- 4 - Bacterial density regulation counterbalances substrate accessibility regulation
- 5 - Regulation of decomposition by bacterial density is more acute for oligotrophs

Journal Pre-proof

Declaration of interests

The authors declare that they have no known competing financial interests or personal relationships that could have appeared to influence the work reported in this paper.

The authors declare the following financial interests/personal relationships which may be considered as potential competing interests:

Journal Pre-proof